2.03 Phase Transitions and Mineralogy of the Lower Mantle

T Irifune and T Tsuchiya, Ehime University, Matsuyama, Japan; Tokyo Institute of Technology, Tokyo, Japan

2.03.1 Introduction

Until recently, experimental high-pressure mineral physics studies mainly focused on materials in the upper part of the mantle because of technical restrictions in pressure and temperature generation and also in precise measurements of crystal structures and physical properties under the lower mantle conditions. However, developments in technologies of both laser-heated diamond anvil cell (LHDAC) and large-volume Kawai-type multianvil apparatus (KMA), combined with synchrotron radiation, have enabled us to quantitatively study phase transitions and some key physical properties of mantle minerals under the *P*, *T* conditions encompassing those of the whole mantle.

Progress in computational mineral physics based on ab initio calculations has also been dramatic in the last two decades in conjunction with the rapid advancement of computer technologies. Classical molecular dynamics calculations required a priori assumptions about the parameters for interatomic model potentials, which largely rely on available experimental data. Quantum mechanical Hamiltonians of many-body electron systems can be efficiently and quantitatively evaluated on the basis of the density functional theory (DFT) (Hohenberg and Kohn, 1964; Kohn and Sham, 1965). Practical calculations of minerals that have complex crystal structures can be achieved using various methods and techniques developed following the DFT. As a result of such advancement in ab initio calculations, it is now possible to predict stability and some physical properties of high-pressure forms quantitatively with uncertainties that are comparable to those in experimentally derived data, as was dramatically shown in a series of recent articles related to the postperovskite (PPv) phase transition (Iitaka et al., 2004; Oganov and Ono, 2004; Tsuchiya et al., 2004a,b).

Another reason for the relatively scarce mineral physics studies for the lower part of the mantle may originate from the fact that there has been no indication of the occurrence of

major phase transitions under these conditions, except for those corresponding to the uppermost (~660–800 km) and lowermost (~2700–2900 km; the D″ layer) parts of the lower mantle. This is in marked contrast to the nature of the mantle transition region, best described as 'the key to a number of geophysical problems' by Birch (1952). Recent seismological studies, however, demonstrated that there are regions that significantly scatter seismic waves, which may be related to some unknown phase transitions and/or chemical boundaries at certain depths in the upper to middle regions of the lower mantle (e.g., Niu and Kawakatsu, 1996). In addition, both geochemical considerations and mantle dynamics simulations suggest that the mantle may be divided into chemically distinct regions by a boundary at a depth of 1500–2000 km in the lower mantle (e.g., Kellogg et al., 1999; Tackley, 2000; Trampert et al., 2004). Moreover, seismological studies with various methods of analysis have shown detailed structures in the D″ layer, demonstrating marked heterogeneity in both horizontal and vertical directions (Lay et al., 2004). Thus, there is growing evidence that the lower mantle is not featureless any more, and many mineral physicists have started to develop experimental and computational techniques for higher pressure and temperature conditions (with improved accuracy) in order to elucidate the mineralogy of the lower mantle.

In spite of the great efforts in both experimental and theoretical studies (mostly conducted in the last two decades), our knowledge of the stability and mineral physics properties of high-pressure phases relevant to the lower mantle is still very limited compared with that of the shallower parts of the mantle. Although LHDACs are now capable of generating pressures and temperatures corresponding to those of the central region of the Earth's interior (Tateno et al., 2010), there remain a number of disagreements in phase equilibrium studies using this method with various techniques in heating, temperature/pressure measurements, phase identification, and so on. Mineral physics parameters that constrain densities of high-pressure phases in the lower mantle have been defined thanks to intense synchrotron sources, particularly those available at third-generation synchrotron facilities, such as ESRF, APS, and SPring-8, combined with both LHDAC and KMA, but those related to elastic wave velocities are scarce to date.

In this chapter, we briefly review recent progress and limitations in experimental and computational techniques in studying phase transitions and some key physical properties under the lower mantle conditions. Then, we summarize current knowledge of these properties obtained experimentally and/or theoretically using these techniques. We focus on the phase transitions and phase relations in simple silicates, oxides, carbonates, and hydrous systems closely related to the mantle and slab materials, because experimental measurements or theoretical predictions of other properties such as shear moduli and their pressure/temperature dependency are still limited, particularly for the conditions of the deeper regions of the lower mantle. In contrast, equation of state (EoS) parameters, that is, zero-pressure densities, bulk moduli, and the pressure/temperature dependencies of some of the high-pressure phases, are summarized as far as reliable data are available. We also review the phase transitions and density changes in lithologies associated with the subduction of slabs and also those in the surrounding model mantle materials on the basis of experimental results on multicomponent systems. Some implications for the mineralogy of the lower mantle are discussed based on these data and those obtained for the simpler systems.

2.03.2 Experimental and Theoretical Backgrounds

2.03.2.1 High-Pressure Technology

Two kinds of high-pressure devices, LHDAC and KMA, have been used to realize static high-pressure and high-temperature conditions of the lower mantle in the laboratory. The upper limit of high-pressure generation in LHDAC has been dramatically expanded using a smaller anvil top (culet) with various shapes for utilizing the potential hardness of a single-crystal diamond. As a result, pressures of multi-megabars can now be comfortably generated in many laboratories. Moreover, quasihydrostatic pressures can be generated by introducing gas pressure media, such as Ar or He, which also serve as thermal insulators when heating samples with laser beams (**Chapter 2.12**).

The quality of heating of samples in LHDAC has also been substantially improved using various laser sources, such as YAG, CO_2, and YLF, with higher powers and more sophisticated computer-controlled feedback systems, as compared with laser heating in the early stages of its development during the 1970s and 1980s. These can now yield a stable high temperature in a sample as small as several tens of micrometers in diameter and even less thickness.

Pressures produced in KMA studies (Kawai and Endo, 1970) using conventional tungsten carbide anvils have long been limited to 25–30 GPa, although the relatively large sample volume in this apparatus made it possible to precisely determine the phase transitions, some physical properties, melting temperatures, element partitioning, etc., of high-pressure phases. Temperatures up to 3000 K are also produced stably for hours or even a few days using various forms of heaters, such as C, $LaCrO_3$, TiC, WC, and some refractory metals. In addition, both temperature and pressure gradients within the sample in KMA are believed to be far smaller than those in LHDAC.

Introduction of harder materials, that is, sintered bodies of polycrystalline diamonds (SD) with some binders, such as Co and Si, as the second stage anvils of KMA has dramatically changed this situation. Using relatively large SD anvil cubes of over 10 mm in edge length, pressures approaching 100 GPa are now produced in some laboratories using KMA (e.g., Ito, 2012; Ito et al., 2005; Tange et al., 2008), without sacrificing the advantage of the relatively large sample volumes in this apparatus. However, the limitations in hardness of SD, as compared to those of pure diamond, should restrict their use as anvils up to around this pressure. On the other hand, nanopolycrystalline diamond (NPD) converted directly from graphite at high pressure and temperature was found to be far harder than SD, and even harder than single crystal diamond (Irifune et al., 2003). The NPD rod samples as large as 1 cm in both diameter and length are now produced on a routine basis (Irifune et al., 2013), which may provide novel anvil material for higher pressure generation in KMA.

Applications of synchrotron radiation to both LHDAC and KMA started in the mid-1980s, when the second-generation

synchrotron sources became available worldwide (e.g., Shimomura et al., 1984). A combination of white x-ray and an energy-dispersive system has been used for KMA experiments at synchrotron facilities, because geometrical constraints imposed by the tungsten carbide anvils and surrounding guide-block systems make it difficult to conduct angle-dispersive diffraction measurements. Use of the energy-dispersive method combined with a multichannel analyzer has the merit of rapid acquisition and analysis of x-ray diffraction data, so that real-time observations of phase transitions are possible under high pressure and high temperature. Although this method is not very suitable for the precise determination of crystal structures (due to relatively low spatial resolutions in the diffraction peak position and also to significant variations in background x-ray with the energy range), some attempts have been successfully made to make crystal structure refinements using combined step scanning and energy-dispersive measurements (Wang et al., 2004). Moreover, developments of an imaging plate (IP) detector and, more recently, x-ray CCD camera (e.g., Hamaya et al., 1996) combined with high-energy monochromatic x-ray allows us to quickly acquire x-ray diffraction from the sample in KMA with an angle-dispersive method, leading to precise diffraction measurements with relatively short acquisition time.

Identification of the phases present and precise determinations of the lattice parameters, and hence unit-cell volumes, of the high-pressure phases can be made by in situ x-ray diffraction measurements. The in situ pressure can also be monitored by the unit-cell volume changes in some reference materials, such as NaCl, Au, Pt, and MgO, using an appropriate EoS. Thus, the phase boundaries and the P, V, T relations of a number of high-pressure phases relevant to lower mantle mineralogy have been determined by in situ x-ray measurements using KMA, although there remain some uncertainties in the estimated pressures due to the lack of reliable pressure scales, as reviewed later, particularly at the pressures of the deeper parts of the lower mantle. The effect of pressure on the electromotive force of a thermocouple is another unresolved issue, which may yield an additional uncertainty in the pressure estimation based on these EoSs.

Corresponding in situ x-ray observations have also been made using LHDAC. As the geometrical restrictions on the x-ray paths are not as severe in this device, x-ray diffraction is measured with an angle-dispersion method using monochromatized x-ray. The x-ray beam is focused to generally ~10–20 μm with collimating mirrors, and directed to the disk-shape sample with diameters of ~20–200 μm, depending on pressure ranges. YAG or ILF lasers with beam sizes of ~10 to several tens μm are used in most of the synchrotron facilities. By adopting IP or x-ray CCD cameras for x-ray exposure combined with data processing systems, rapid data acquisition and reductions are also possible. Thus, the phase identification and measurements of unit-cell parameters of high-pressure phases can be made by the combination of LHDAC and synchrotron radiation at pressure and temperature conditions corresponding to the entire mantle (e.g., Murakami et al., 2004a) and even to the inner core (e.g., Tateno et al., 2010).

The major uncertainty in the in situ x-ray observations with LHDAC arises from the possible large temperature gradients in the small thin sample. Some studies demonstrated that variations of temperature are not very large in the radial direction of the disk-shape sample, suggesting that the temperature uncertainty may be on the order of ~10% or less of the nominal values if the diameter of the laser beam is significantly larger than that of the x-ray beam (Shen et al., 2001). However, the temperature gradient in the axial direction of the sample can be substantially larger than this estimation (Irifune et al., 2005), depending on the nature and thickness of the thermal insulator or pressure medium, as diamond has very high thermal conductivity. Efforts have been made to overcome this issue by either coating the sample with some metal of high thermal conductivity (Sinmyo et al., 2008) or using 'nano-beams' far less than 100 nm (e.g., Ice et al., 2010) to reduce the effects of thermal gradients in the sample.

2.03.2.2 Ab Initio Calculation

Ab initio approaches are those that solve the fundamental equations of quantum mechanics with a bare minimum of approximations. DFT is, in principle, an exact theory for the ground state and allows us to reduce the interacting many-electron problem to a single-electron problem (the nuclei being treated as an adiabatic background). A key to the application of DFT in handling the interacting electron gas was given by Kohn and Sham (1965) by splitting the kinetic energy of a system of interacting electrons into the kinetic energy of noninteracting electrons plus some remainder, which can be conveniently incorporated into the exchange-correlation energy.

The local density approximation (LDA) (Kohn and Sham, 1965) replaces the exchange-correlation potential at each point with that of a homogeneous electron gas with a density equal to the local density at the point. The LDA works remarkably well for a wide variety of materials, especially in the calculations of equations of state, elastic constants, and other properties of silicates. Cell parameters and bulk moduli obtained from well-converged calculations often agree with the experimental data within a few percent and ~10%, respectively. Agreement with the laboratory data is not perfect, however, and some systematic discrepancies are noted for some materials.

Attempts to improve LDA via introducing nonlocal corrections have yielded some success. The generalized gradient approximation (GGA) (Perdew et al., 1992, 1996) is a significantly improved method over LDA for certain transition metals (Bagno et al., 1989) and hydrogen bonded systems (Hamann, 1997; Tsuchiya et al., 2002, 2005a). There is some evidence, however, that GGA improves the energetics of silicates and oxides but the structures can be underbound. The volume and bulk moduli calculated with GGA tend to be larger and smaller, respectively, than those measured experimentally (Demuth et al., 1999; Hamann, 1996; Tsuchiya and Kawamura, 2001). Considering the thermal effect with zero-point motion, LDA provides the structural and elastic quantities much closer (typically within a few percent) to experimental values than those obtained with GGA. In addition, a discrepancy of about 10–15 GPa is usually seen in transition pressures calculated with LDA and GGA (Hamann, 1996; Tsuchiya et al., 2004a,c), which provide lower and upper bounds, respectively. Experimental transition pressures are usually found between the values obtained with LDA and GGA, although GGA tends to provide the pressure with better fit to the experimental value than LDA (Hamann, 1996; Tsuchiya et al., 2004a,c). The main

source of computational error can be attributed to how to treat the exchange-correlation potential.

The standard DFT has limitations in applying to Fe-bearing oxides and silicates in the following case. One-electron approximation with the standard DFT approaches fails to describe the electronic structure of Fe–O bonding correctly due to its strongly correlated behavior. Both LDA and GGA usually produce metallic bands for Fe–O bonding in silicates. They also do not provide the correct crystal field effects that break the d orbital degeneracy. More sophisticated classes of technique, such as LDA+U, LDA+DMFT (dynamical mean-field theory), multireference configurational interaction, etc. are needed to treat the many-body effect of electrons more accurately and to investigate geophysically important iron-bearing systems.

Among these schemes, LDA+U (Anisimov et al., 1991) is the most practical method for minerals under the current state of computer technology. The main problem of applying LDA+U to materials under pressure is the determination of the effective Hubbard U parameter, meaning screened on-site Coulomb interaction. Tsuchiya et al. (2006), Hsu et al. (2011), and Metsue and Tsuchiya (2011) computed the effective U in magnesiowüstite (Mw) $(Mg_{1-x}Fe_x)O$, perovskite $(Mg_{0.875}Fe^{3+}_{0.125})(Si_{0.875}Fe^{3+}_{0.125})O_3$, and PPv $(Mg_{0.9375}Fe_{0.0625})SiO_3$ in a nonempirical and internally consistent way based on a linear response approach for the occupancy matrix (Cococcioni and de Gironcoli, 2005), respectively.

Combining these techniques, the ab initio lattice dynamics method (Baroni et al., 1987, 2001) and quasiharmonic approximation (Wallace, 1972), the calculation condition was successfully extended to finite temperature including phonon thermodynamics (Karki et al., 2000a,b; Tsuchiya, 2003; Tsuchiya et al., 2004a,c). EoS and other high-temperature properties can now be computed in the whole mantle P, T condition quite accurately, even nonempirically. The density functional perturbation theory (Baroni et al., 1987, 2001) plays a key role there, allowing direct access to the harmonic dynamical matrix. More recently, the technique was further extended to high-temperature properties of iron-bearing systems combined with the internally consistent LDA+U (Fukui et al., 2012; Metsue and Tsuchiya, 2011, 2012; Tsuchiya and Wang, 2013).

Another important new research direction is a technical enhancement in evaluating transport properties. For example, an extension of the harmonic lattice dynamics framework to the anharmonic lattice dynamics enabled access to lattice thermal conductivity of minerals, which is important in understanding the deep mantle thermal property. Dekura et al. (2013) calculated lattice thermal conductivity of $MgSiO_3$ perovskite under the lower mantle P, T conditions for the first time within the third-order level of anhamonicity, and estimated a moderate core–mantle boundary (CMB) heat flow of ~3–6 TW and a Rayleigh number of the lower mantle large enough to drive a vigorous convection. Metsue and Tsuchiya (2013), on the other hand, investigated the shear response of possible slip systems activated in Fe-bearing $MgSiO_3$ PPv based on generalized stacking fault (GSF) energy calculations. Although some computational conditions such as system size or chemical composition are limited in these studies compared to actual systems, this situation will be greatly improved in the near future.

2.03.2.3 Pressure Scale

The construction of an accurate pressure standard is a critical issue in the quantitative measurements of mineral physics properties under high pressure. The pressure (P)–volume (V)–temperature (T) EoS (PVT-EoS) of materials is most useful in evaluating the experimental pressures under the P, T conditions of the Earth's deep mantle. The EoS of a pressure standard is usually derived on the basis of a conversion of dynamical shock Hugoniot data to isothermal compression data. In principle, some parameters specifying the thermal properties of a solid are necessary for this conversion process of the Hugoniot. However, measurements of these parameters without any pressure or temperature standards are virtually impossible. In all EoSs presently used as primary pressure standards, the conversion of the Hugoniot was, therefore, performed with some simple assumptions about the unknown high-pressure behavior of the conversion parameters. The most critical issue on the validity of such assumptions is the volume dependence of the thermodynamic Grüneisen parameter, which is a fundamental quantity characterizing the thermal effect on the material.

The characteristic properties of gold (Au), namely its low rigidity, simple crystal structure, chemical inertness, and structural stability, make it particularly suitable as a pressure standard under high P, T conditions, and it has, therefore, been used as a primary standard in many in situ x-ray diffraction studies (e.g., Funamori et al., 1996; Mao et al., 1991). However, some recent in situ experiments noted that the pressure values estimated by different thermal EoSs of gold show significant discrepancies. Using the EoS of gold proposed by Anderson et al. (1989), which is frequently used as the pressure scale in experiments using multianvil apparatus, Irifune et al. (1998a) first reported that the postspinel phase boundary of Mg_2SiO_4 shifted to about 2.5 GPa lower than the pressure corresponding to the depth of the 660-km seismic discontinuity (~23.5 GPa and ~2000 K). Similar results were obtained for other various minerals as summarized in Irifune (2002).

Tsuchiya (2003) predicted the thermal properties and the PVT-EoS of gold based on the ab initio theory including thermal effect of electrons. The state-of-the-art ab initio calculation showed that the relationship $\gamma/\gamma_0 = (V/V_0)^q$, assumed in some studies, is adequate for gold, at least up to $V/V_0 = 0.7$ and the predicted values of q was 2.15, which is intermediate between the values used in Heinz and Jeanloz (1984) and Anderson et al. (1989). According to this study, the ab initio EoS model reduced the discrepancies between the observed phase boundaries of spinel, ilmenite, and garnet and the seismic discontinuity. However, a gap of about 0.7 GPa still remains between the postspinel transition pressure and that of the 660-km discontinuity. The similar conclusions with a slightly larger (1.0–1.4 GPa) discrepancy has also been obtained by an experimental study using an empirical PVT-EoS model of MgO to determine pressure (Matsui and Nishiyama, 2002).

Even for gold, there are several PVT models, derived by different groups, which are still not mutually consistent. Such a problem is also found in EoSs of platinum (Holmes et al., 1989; Jamieson et al., 1982). Moreover, platinum appears to be unsuitable for the pressure scale in some cases because of its reactivity with the sample or materials of the experimental cell at high P, T conditions (Ono et al., 2005a). A similar problem

is also encountered with the pressures obtained using MgO. The pressures obtained using EoSs of different materials, therefore, show a significant scatter. Akahama et al. (2002) determined the pressures based on room-temperature EoSs of several materials compressed simultaneously in a diamond anvil cell and reported that the EoS of platinum proposed by Holmes et al. (1989) provided pressures more than 10 GPa higher than those calculated using EoS of gold as proposed by Anderson et al. (1989) at pressures of a megabar even at 300 K. A similar inconsistency has also been reported in pressure determination based on gold and silver EoSs (Akahama et al., 2004).

Examples of the difference in pressures based on a different EoS of gold than that of platinum are shown in **Figure 1**, along a temperature (2300 K) close to the typical lower mantle geotherm. The pressures evaluated based on various EoSs of gold differ by ~2–3 GPa at the pressures of the uppermost parts of the lower mantle (25–30 GPa), and are within 5 GPa at pressures up to ~60 GPa. However, the differences become substantially larger at higher pressures, reaching ~15 GPa at the base of the lower mantle (136 GPa). It is also seen that the pressures based on an EoS of Pt (Holmes et al., 1989) are even higher than the highest pressure estimation by Tsuchiya (2003) by 5 GPa at 136 GPa.

An attempt to determine a more accurate and reliable EoS of MgO was made by using unified analyses for available pressure-scale-free experimental data sets, including shock-compression Hugoniot, zero-pressure thermal expansion, high-temperature adiabatic bulk moduli, and room-temperature and high-pressure adiabatic bulk moduli data (Tange et al., 2009a). The resultant EoS successfully reproduced all the data used for the analyses throughout the entire lower mantle P, T conditions, which yields slightly higher pressures than those derived by other EoSs of MgO commonly used for in situ x-ray measurements (Matsui et al., 2000; Speziale et al., 2001). The new EoS of MgO yileds the spinel–postspinel transition pressure of about 22.5 GPa at 2000 K (Tange et al., 2009a) using the experimental data of Fei et al. (2004), which is about 1 GPa lower than the pressure for the 660 km discontinuity. A pressure-scale-free EoS of MgO has also been proposed on the basis of the analyses of ultrasonic sound velocity data combined with unit-cell volume compression data (Kono et al., 2010), which yields pressures consistent with those derived by the above pressure scale at least at pressures to the upper parts of the lower mantle.

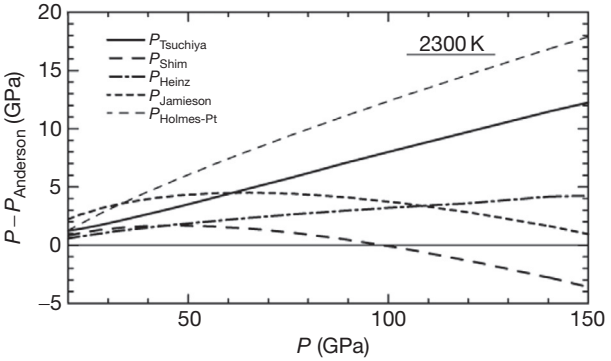

Figure 1 Differences between the pressures calculated using various equation of states (EoSs) of gold (Heinz and Jeanloz, 1984; Jamieson et al., 1982; Shim et al., 2002a; Tsuchiya, 2003) and those based on Anderson et al. (1989, horizontal line) as a function of pressure at 2300 K. The difference between the pressures using the Anderson scale and those using EoS of platinum by Holmes et al. (1989) is also shown for comparison.

2.03.3 Mineral Phase Transitions in the Lower Mantle

2.03.3.1 Major Minerals in the Mantle and Subducted Slab

Phase transitions in Earth-forming materials dominate the structure and dynamics of the Earth. Major changes in seismic velocities traveling through the Earth's mantle can be generally attributed to the phase transitions of the constituent minerals, although some of them may be closely related to some chemical changes. Exploration and investigation of high-pressure phase transitions in mantle minerals have, therefore, been one of the major issues in studying the Earth's deep interior.

Here, we summarize the phase transitions in major minerals under lower mantle conditions. Phase transitions in some relatively minor minerals relevant to the subducted slab lithologies are also reviewed in the following section. As the experimental data on the phase transitions are still limited and controversial at P, T conditions of the lower mantle, we have tried to construct the most likely phase diagrams for the minerals with simple chemical compositions based on available laboratory data and ab initio calculations. Thermoelastic properties of some key high-pressure phases are also reviewed and summarized here, as far as experimental data or theoretical predictions are available.

2.03.3.1.1 $MgSiO_3$

The high-pressure orthorhombic perovskite polymorph of $MgSiO_3$ (Mg-Pv) is believed to be the most abundant mineral in the Earth's lower mantle. The possibility of a further phase transition of this phase under the lower mantle P, T conditions has been controversial: Some studies suggest that Mg-Pv dissociates into an assemblage of SiO_2 and MgO at 70–80 GPa and 3000 K (Meade et al., 1995; Saxena et al., 1996) or that it undergoes a subtle phase change above 83 GPa and 1700 K (Shim et al., 2001b), while others claimed Mg-Pv is stable almost throughout the lower mantle (e.g., Fiquet et al., 2000). However, more recent studies suggest that the result of Shim et al. (2001b) was due to misidentification of the diffraction peaks of a newly formed platinum carbide (Ono et al., 2005a). The dissociation of Mg-Pv into the oxides is also unlikely to occur in the Earth's mantle according to the subsequent experimental (Murakami et al., 2004a, 2005; Oganov and Ono, 2004) studies. Theoretical investigations also suggest the dissociation should occur at extremely high pressure above 1 TPa (Tsuchiya and Tsuchiya, 2011b; Umemoto et al., 2006).

Recently, the Pv to PPv transition in $MgSiO_3$ was found to occur by in situ x-ray diffraction experiment using LHDAC and ab initio calculations at ~2500 K and ~125 GPa (Murakami et al., 2004a; Oganov and Ono, 2004; Tsuchiya et al., 2004a; **Figure 2**), close to the P, T conditions of the D″ layer near the CMB. The Mg-PPv phase has a crystal structure identical to that of $CaIrO_3$ with a space group *Cmcm*. This structure consists of

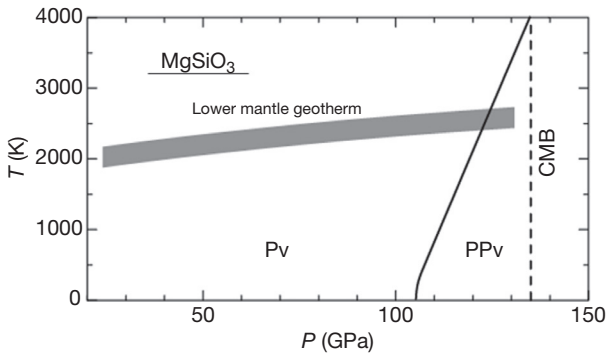

Figure 2 High P, T phase diagram for $MgSiO_3$ at lower mantle pressures summarized based on the laser-heated diamond anvil cell (LHDAC) experiments by Murakami et al. (2004a) and ab initio calculations by Tsuchiya et al. (2004a). Shaded area represents a typical lower mantle geotherm based on Brown and Shankland (1981). Pv, perovskite; PPv, postperovskite; CMB, core–mantle boundary.

silica layers stacking along the b direction and intercalated Mg ions. In the silica layers, SiO_6 octahedra connect sharing edges along the a direction and sharing corners along the c direction. Thus, this structure is more favorable at high pressure than the Pv structure, although the cation coordinations are basically the same in both structures.

The PPv structure is expected to be highly anisotropic. It is more compressible along the b direction perpendicular to the silica layers because only ionic Mg–O bonding exists in the interlayer spacing. The Pv and PPv structures, therefore, look very different in this respect. However, the structural relationship between Pv and PPv is quite simple and by applying shear strain ε_6, Pv can change to PPv directly (Tsuchiya et al., 2004a). According to this relation, the c direction remains unchanged via the structural transition. This suggests that nonhydrostaticity could significantly affect the transition kinetics of the Pv to PPv transition.

PPv's thermodynamic properties and the position and slope of the phase boundary were investigated by means of ab initio quasiharmonic free energy calculations (Tsuchiya et al., 2004a, 2005b). The predicted Clapeyron slope of the Pv–PPv transition was ~7.5 MPa K^{-1}, which is remarkably close to that required for a solid–solid transition to account for the D″ discontinuity (Sidorin et al., 1999). Thus, the results of both experimental and theoretical studies suggest that the PPv should be the most abundant high-pressure phase in the D″ region.

Over the past decades, there have been a number of experiments to determine the elastic property of Mg-Pv (e.g., Fiquet et al., 2000; Funamori et al., 1996; Mao et al., 1991; Ross and Hazen, 1990; Yagi et al., 1982; Yeganeh-Haeri et al., 1989). Among these experiments, early studies yielded relatively large variations for zero-pressure bulk modulus K_0 of Mg-Pv ranging from 254 (Ross and Hazen, 1990) to 273 GPa (Mao et al., 1991). However, more recent experiments of static compression and Brillouin spectroscopy yielded mutually consistent K_0 values of ~253–264 GPa. Density functional calculations have reported similar but slightly smaller room-temperature bulk modulus for Mg-Pv of about 250 GPa (Tsuchiya et al., 2004b, 2005b; Wentzcovitch et al., 2004). This underbinding tendency for Mg-Pv is seen in standard DFT calculations but is much more prominent in GGA than in LDA (Wentzcovitch et al., 2004).

In contrast to the extensive investigations of the EoS of Mg-Pv, the EoS of Mg-PPv has not been well constrained experimentally. According to a density functional prediction, the zero-pressure volume of Mg-PPv is very close to that of Mg-Pv (Tsuchiya et al., 2004a, 2005b). However, K_0 and its pressure derivative of Mg-PPv are significantly smaller and larger than those of Mg-Pv, respectively, which implies the volume of Mg-PPv should be smaller than that of Mg-Pv at the relevant pressure range. The volume decrease associated with the Pv–PPv transition is estimated to be ~1.5% on the basis of ab initio calculations (Tsuchiya et al., 2004a), which is consistent with those estimated based on LHDAC experiments.

2.03.3.1.2 $MgSiO_3$–$FeSiO_3$

Mg-Pv is supposed to incorporate 5–10 mol% of $FeSiO_3$ in peridotitic compositions in the lower mantle (Irifune, 1994; Katsura and Ito, 1996; Wood and Rubie, 1996). However, experimental studies for the system $MgSiO_3$–$FeSiO_3$ have been limited to the pressures of the uppermost part of the lower mantle, except for a LHDAC study (Mao et al., 1991). Recent developments in KMA with sintered diamond anvils substantially extend the pressure and temperature ranges for phase equilibrium studies as reviewed earlier, and Tange et al. (2009b) extensively studied the phase relations and the Mg–Fe partitioning between coexisting Mg-Pv and Mw at pressures up to ~50 GPa and temperatures to 2300 K.

Immediately after the discovery of the Pv–PPv transition in $MgSiO_3$, the effects of iron on this transition were studied using LHDAC (Mao et al., 2004, 2005). It was noted that the presence of iron significantly reduce the stability pressure of PPv, and PPv with up to ~80 mol% of the $FeSiO_3$ component synthesized at a pressure of ~140 GPa and at temperatures of ~2000 K (Mao et al., 2005). However, subsequent studies (Andrault et al., 2010; Hirose et al., 2008; Sinmyo et al., 2008; Stixrude and Lithgow-Bertelloni, 2011; Tateno et al., 2007) suggest that the presence of ferrous iron increases the stability pressure of PPv, contrary to this study. Thus, the phase relations in the system $MgSiO_3$–$FeSiO_3$ at pressure up to ~130 GPa and at a typical lower mantle temperature can be drawn as illustrated in **Figure 3**, according to the results of these more recent studies, although the phase boundaries at pressures higher than 50 GPa have not been well constrained.

A large Pv+PPv coexisting pressure range of ~20 GPa was observed for the $(Mg_{0.9}Fe_{0.1})SiO_3$ composition (Catalli et al., 2009), but the multicomponent phase boundary determined by the LHDAC technique in the Mbar condition suffers substantial uncertainty. On the other hand, a significant effect of ferrous iron on the stability of Mg-PPv has also been predicted by some theoretical works using GGA (Caracas and Cohen, 2005b; Stackhouse et al., 2006). However, this technique is known to be less applicable to the iron-bearing system as mentioned earlier. In contrast, a recent internally consistent LDA+U+ab initio LD+QHA study showed much smaller effects even at mantle temperatures (Metsue and Tsuchiya, 2012), being consistent with a different LHDAC experiment (Sinmyo et al., 2008). These calculations, particularly Tsuchiya and Wang (2013), also reported that a Pv dominant

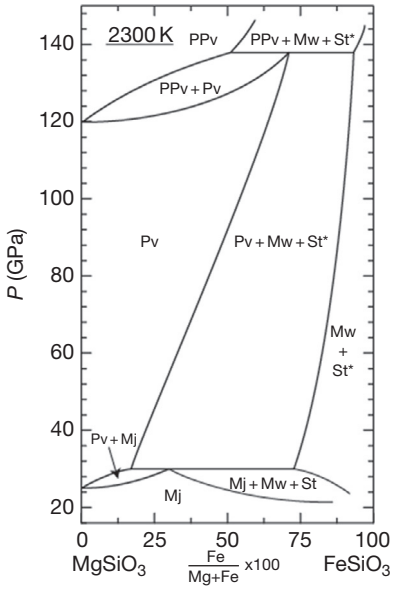

Figure 3 A predicted phase diagram for the system $MgSiO_3$–$FeSiO_3$ at lower mantle pressures and at a representative lower mantle temperature (2300 K). The relations below ~30 GPa are estimated on the basis of Sawamoto (1987) and Ohtani et al. (1991) using Kawai-type multianvil apparatus (KMA), while those above 80 GPa are based on LHDAC experiments by Tateno et al. (2007) and Hirose et al. (2008) but may suffer substantial uncertainties in the phase boundaries. The boundaries between these pressures are depicted based on recent experimental data using KMA with SD anvils (Tange, 2009a). Mj, majorite garnet; Mw, magnesiowüstite; St, stishovite; *stishovite, $CaCl_2$-type or α-PbO_2-type phases, depending on pressure.

composition cannot reproduce seismological observations of the lower mantle. This is qualitatively consistent with an EoS measurement of Pv (Tange et al., 2012), but less supportive of a Brillouin scattering experiment (Murakami et al., 2012).

The effect of iron on the PPv transition has also been studied in the light of the high-pressure phase changes of hematite, corundum-type Fe_2O_3. Hematite transforms first to the high-pressure phase with the *Pbnm* Pv structure or Rh_2O_3(II) structures at 30 GPa, whose x-ray diffraction patterns are very similar to each other (Ono et al., 2005b). Further transitions in Fe_2O_3 to the structure assigned as the $CaIrO_3$-type structure has been reported to occur at a transition pressure of ~50 GPa (Ono et al., 2005b). This transition pressure is significantly lower than the Pv–PPv transition pressure in $MgSiO_3$. Thus, the presence of iron in the trivalent state is also suggested to lower the pressure of the Pv–PPv transition, unlike divalent ferrous iron. Nevertheless, this issue has not been fully resolved and there remains a lot of room for further theoretical and experimental investigation.

2.03.3.1.3 $MgSiO_3$–Al_2O_3

Irifune (1994) demonstrated that Mg-Pv is the major host of aluminum in a pyrolite composition at pressures and temperatures of the uppermost parts of the lower mantle, possessing ~4 mol% of Al_2O_3. Phase relations in the system $MgSiO_3$–Al_2O_3 under the lower mantle conditions have since been studied (Irifune et al., 1996a; Ito et al., 1998) with an emphasis on the $MgSiO_3$–$Mg_3Al_2Si_3O_{12}$ system. Irifune et al. (1996a) showed that majorite garnet with less than ~15 mol% Al_2O_3 transforms to the Pv structure via a mixture of these two phases, while this assemblage further changes to an assemblage of majorite plus corundum at pressures about ~28 GPa, at 1800 K. This assemblage with the $Mg_3Al_2Si_3O_{12}$ composition was later shown to form almost pure Pv at ~38 GPa using KMA with SD anvils (Ito et al., 1998).

Phase transitions in Al_2O_3 corundum under the lower mantle condition were first studied by Funamori and Jeanloz (1997) using LHDAC based on earlier ab initio predictions (Marton and Cohen, 1994; Thomson et al., 1996), which demonstrated that corundum transforms to a new phase with the Rh_2O_3 (II) structure at ~100 GPa and at ~1000 K. More recently, it has been predicted by ab initio studies that Al_2O_3 has a similar high-pressure phase relation to Fe_2O_3 (Caracas and Cohen, 2005a; Stackhouse et al., 2005b; Tsuchiya et al., 2005c). The Pv to PPv transition was thus suggested to occur in Al_2O_3 at about 110 GPa at 0 K, although the Pv phase is eclipsed by the stability field of the Rh_2O_3(II) phase. This Pv to PPv transition pressure in Al_2O_3 is about 10 GPa higher but fairly close to that in $MgSiO_3$, though Akber-Knutson et al. (2005) predicted a much larger effect of Al by estimating the solid solution energy. In contrast to these static-temperature calculations, a more careful modeling for finite temperature, solid-solution phase equilibria based on the statistical mechanical multi-configuration sampling approach (Tsuchiya and Tsuchiya, 2008) indicated a much smaller effect of aluminum. A narrow Pv+PPv coexisting pressure width expected for the reasonable Al content in the lower mantle could be responsible for the observations of the sharp D″ discontinuity (Lay et al., 1998).

In situ x-ray diffraction experiments on pyrope compositions by LHDAC (Tateno et al., 2005) demonstrated a consistent result regarding the effect of aluminum incorporation on the PPv transition pressure. Andrault et al. (2010) also reported a large Pv+PPv coexisting region from ~120 to ~150 GPa in the peridotitic Al and Fe composition and from ~100 to ~180 GPa in a more felsic composition by LHDAC. The broad coexisting region was similarly observed by LHDAC (Catalli et al., 2009; Nishio-Hamane et al., 2007), although the pressure intervals of the coexisting regions are inconsistent in these studies. For instance, Nishio-Hamane et al. (2007) reported that the coexisting region starts from ~150 GPa and ends at ~170 GPa in the similar composition, which is substantially higher than those of other studies and even higher than the CMB pressure (136 GPa). These conflicting results show that the accurate determination of the multicomponent phase boundary is difficult for the Mbar region using current LHDAC techniques. Thus, we rely on the theoretical results and expect that the effect of aluminum on the PPv transition pressure in $MgSiO_3$ is not very significant. The plausible phase diagram of the system $MgSiO_3$–Al_2O_3 in the lower-mantle *P*, *T* condition is illustrated in **Figure 4**.

The presence of Al_2O_3 in Fe-bearing Pv is known to lead to a coupled substitution of Fe^{3+} and Al^{3+} for Mg^{2+} and Si^{4+} in Pv (Frost and Langenhorst, 2002; McCammon, 1997; Wood and Rubie, 1996), yielding substantial enrichment of ferric iron in Pv in the uppermost regions of the lower mantle (Irifune, 1994; Irifune et al., 2010; Nishiyama and Yagi, 2003; Wood, 2000). In addition to this coupled substitution effect, it has

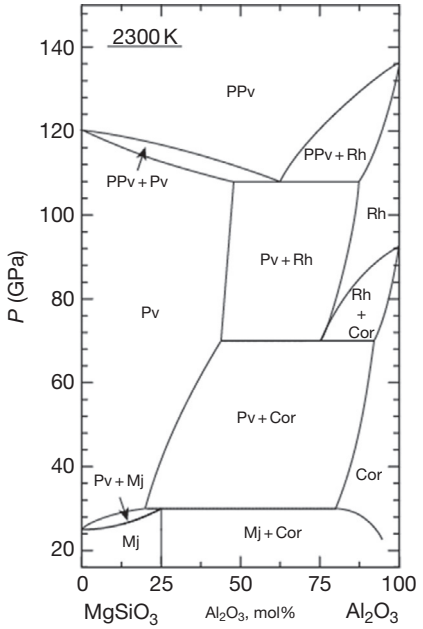

Figure 4 A predicted phase diagram for the system $MgSiO_3$–Al_2O_3 at lower mantle pressures and at 2300 K. The phase relations below ~40 GPa are based on KMA experiments (Irifune et al., 1996a; Ito et al., 1998), while those on Al_2O_3 are from Funamori et al. (1998) using LHDAC and ab initio calculations by Tsuchiya et al. (2005c). The boundaries at 120–130 GPa are based on a theoretical prediction by Tsuchiya and Tsuchiya (2008). Cor, corundum; Rh, Rh_2O_3(II).

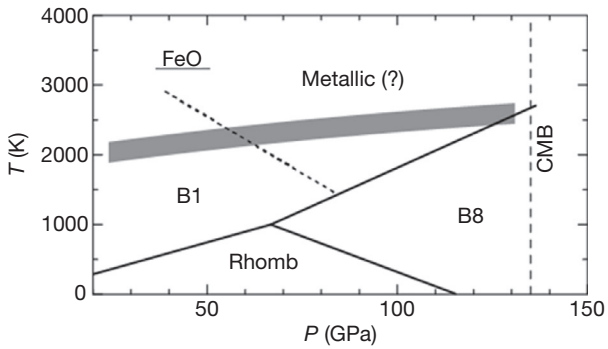

Figure 5 High *P*, *T* phase diagram for FeO at lower mantle pressures summarized based on the in situ measurement by Fei and Mao (1994), Murakami et al. (2004b), and Kondo et al. (2004). The *P*, *T* boundary above which metallization in FeO is reported to occur (Ohta et al., 2012) is shown by the dotted line. B1, NaCl structure; B8, NiAs structure; Rhomb, rhombohedral B1 phase.

been suggested that the high-spin to low-spin transitions in both Pv and Mw may cause some significant changes in the partitioning of iron between these major phases in the lower mantle. Although the nature of the spin transition in Mw has been fairly well understood based on recent ab initio computations and experimental studies (see below), those in Pv have not yet been resolved. This is partly because Pv has two cation sites (A and B) and can accommodate both ferrous and ferric irons, depending on the alumina content, which makes the computational and experimental studies extremely difficult. The current situations on the studies of spin transitions in Pv can be seen in a recent comprehensive review article (Lin et al., 2013), which, however, may suffer some significant revisions in the near future, considering the rapid progress in this research field.

2.03.3.1.4 MgO–FeO

Mw, $(Mg_{1-x}Fe_x)O$, is believed to be the next major mineral phase in Earth's lower mantle after ferrosilicate Pv $(Mg_{1-x}Fe_x)SiO_3$ (e.g., Helffrich and Wood, 2001). The magnesium end-member of Mw, periclase, possessing the B1 (NaCl) structure, is known to be an extraordinarily stable phase. No phase transitions in this material have been observed or predicted under the *P*, *T* conditions of the entire mantle (Alfé et al., 2005; Duffy et al., 1995), primarily due to substantially smaller ionic radius of magnesium relative to that of oxygen. FeO wüstite, on the other hand, transforms to an antiferromagnetic phase accompanied by a small rhombohedral distortion. This transition is a typical magnetic order–disorder transition and, therefore, the transition temperature corresponds to the Neel point. Although the rhombohedral B1 (rB1) phase is stable at low temperatures up to about 110 GPa, at higher pressure over 65 GPa and high temperatures, the rB1 phase transforms to the normal or inverse B8 (NiAs) structure, as shown in **Figure 5** (Fei and Mao, 1994; Kondo et al., 2004; Murakami et al., 2004b). However, several important properties of this high-pressure phase, such as high-temperature stability, structural details, and electronic property, are still in debate (Fei and Mao, 1994; Mazin et al., 1998; Murakami et al., 2004b).

For the compositions between the two end-members of MgO and FeO, some controversial experimental results have emerged: Mw with $X_{Fe} = 50\%$ was reported to dissociate into two components, Fe-rich and Mg-rich Mws at 86 GPa and 1000 K (Dubrovinsky et al., 2000). In contrast, another study using LHDAC found no dissociation of Mw with even higher X_{Fe} of 61% and 75% up to 102 GPa and 2550 K, though the sample with $X_{Fe} = 75\%$ showed a displacive transition to the rB1 structure at low temperature similar to FeO wüstite (Lin et al., 2003). Thus, further experimental and theoretical studies are required to address the possible dissociation of Mw.

It has been demonstrated that FeO with the B1 structure suffers metallization under the *P*, *T* conditions of the lower mantle (**Figure 5**) on the basis of electric conductivity (Ohta et al., 2010, 2012) and radiometric (Fischer et al., 2011) measurements, as well as first principles calculations (Ohta et al., 2012). Metallization of FeO suggests that oxygen may be readily incorporated into the Earth's core as the major alloying light element with some important geochemical implications (Ringwood et al., 1990). Moreover, the possible existence of the iron-rich Mw in the lowermost mantle (e.g., Wicks et al., 2010) should lead to strong electromagnetic interactions with the liquid outer core if such Mw is of metallic nature.

Another issue relevant to Mw, as well as the ferrosilicate Pv, which should affect the thermoelastic properties of these phases, is the occurrence of electron spin transitions under the lower mantle conditions. High spin (HS) to low spin (LS) transitions in iron have been observed by in situ x-ray emission spectroscopy and Mössbauer spectroscopy from 40 to 70 GPa in Mw containing about 18% iron (Badro et al., 2003; Lin et al., 2005) and from 70 to 120 GPa in $(Mg,Fe)SiO_3$ Pv

(Badro et al., 2004; Jackson et al., 2005; Li et al., 2004) at room temperature. Several significant effects of the thermochemical state of the lower mantle can be inferred by the spin transition of iron. The spin transition in Mw is accompanied by significant volume reductions (Lin et al., 2005; Tsuchiya et al., 2006) and changes in these minerals' optical absorption spectrum (Badro et al., 2004). These can produce (1) seismic velocity anomalies, (2) variations in $Mg–Fe^{2+}$ partitioning between Mw and Pv, (3) changes in radiative heat conductivity, and (4) compositional layering (Badro et al., 2003, 2004; Gaffney and Anderson, 1973). The elastic signature of this transition in Mw has been partially explored (Lin et al., 2005), but there is still much uncertainty. In contrast, anomalous compression behavior has not yet been observed in $(Mg,Fe)SiO_3$ Pv.

The strongly correlated behavior of iron oxide has deterred the quantification of these changes by density functional calculations based on the local spin density approximation and spin polarized generalized gradient approximation (σ-GGA). These approaches incorrectly predict a metallic HS ground state and then successive spin collapses across the transition as reported for FeO (Cohen et al., 1997; Sherman and Jansen, 1995). More recently, a new model explaining the mechanism of HS-to-LS transition of iron in Mw has been proposed based on calculations using a more sophisticated LDA+U technique that describes the electronic structure of a strongly correlated system more correctly (Tsuchiya et al., 2006). In this study, the effective Hubbard U parameter has been optimized at each volume and at each iron concentration up to X_{Fe} of 18.75% in an internally consistent way. As a result, it has been demonstrated that the large stability field of HS/LS mixed state appears at high temperatures instead of the intermediate spin state, due to the contributions of coexisting HS/LS mixing entropy and magnetic entropy. According to this transition mechanism, Mw is expected to be in this HS/LS mixed state for almost the entire range of lower mantle P, T conditions with the proportion of HS iron decreasing continuously with increasing pressure (**Figure 6**). No discontinuous change in any physical properties would appear to be associated with the spin transition in Mw within this range. Although phonon effects were neglected to calculate the high-temperature energetics in Tsuchiya et al. (2006), these effects were later examined by the internally consistent LDA+U+ab initio LD+QHA calculations (Fukui et al., 2012), which demonstrated that the effects are indeed unchanged across the spin transition and thus negligible in calculating the finite-temperature mixed spin (MS) region at least for the $(Mg_{0.875}Fe_{0.125})O$ composition.

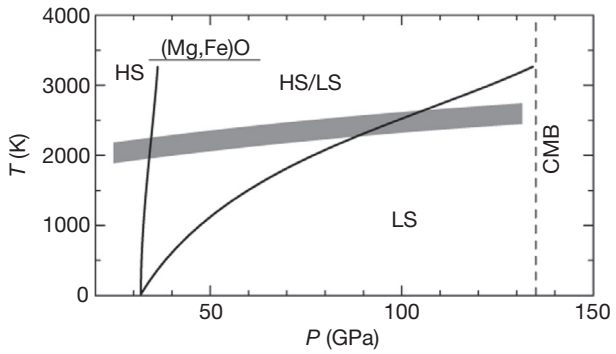

Figure 6 High P, T spin transition diagram for Mw with iron concentration of 18.75% at lower mantle pressures predicted on the basis of LDA+U calculations by Tsuchiya et al. (2006). HS, high spin; LS, low spin.

It has been reported that the spin transition pressure significantly increases with increasing X_{Fe}. A volume decrease associated with the spin transition was observed in $(Mg_{0.4}Fe_{0.6})O$ at 95 GPa (Lin et al., 2005), while no spin transition has so far been reported in pure FeO up to 143 GPa (Badro et al., 1999). Iron–iron interactions, which are no longer negligible at X_{Fe} higher than 20%, might also reinforce the magnetic moment significantly, although the mechanism of this tendency has not been fully understood to date.

Some studies propose anomalous behaviors in the MS state of Mw for elasticity (Crowhurst et al., 2008; Marquardt et al., 2009a; Wentzcovitch et al., 2009), electrical conductivity (Lin et al., 2007), and viscosity (Wentzcovitch et al., 2009). These, however, currently lack corroborative evidence. In contrast, other experiments observed no, or marginal, anomalies in the elasticity of Mw (Antonangeli et al., 2011; Murakami and Bass, 2011). Although further investigations are clearly required for detailed understanding, the latter seems physically reasonable if the MS state is considered to be a kind of two-phase coexistence.

It is also pointed out that the spin crossover in Mw affects its elastic anisotropy (Marquardt et al., 2009b). LS Mw was reported to have at least 50% stronger shear anisotropy in the lowermost mantle compared to MgO, which is originally quite anisotropic at high pressures (Karki et al., 1999; Tsuchiya and Kawamura, 2001). According to this result, Mw was inferred to be a dominant cause of seismic anisotropy in the D″ layer (Marquardt et al., 2009b), but careful modeling of the rheological property, including both PPv and Mw, is obviously required to analyze the source of observed anisotropy in more detail (Merkel et al., 2007; Metsue and Tsuchiya, 2013; Miyagi et al., 2010).

2.03.3.1.5 $CaSiO_3$

The lower mantle is believed to consist mainly of $(Mg,Fe)SiO_3$ Pv and Mw, with some $CaSiO_3$ perovskite (Ca-Pv) up to 7–8 vol% (e.g., Irifune, 1994). Despite its importance, there are many unanswered questions about the structure, stability, EoS, and other physical properties of Ca-Pv under pressure and temperature, which complicate some attempts to model the mineralogy of the lower mantle (e.g., Stacey and Isaak, 2001).

$CaSiO_3$ crystallizes to the Pv structure over 10–13 GPa, depending on temperature, and is known to be unquenchable at ambient conditions. At lower mantle conditions, $CaSiO_3$ has an ideal cubic Pv structure, while, at lower temperatures, it is suggested to be slightly distorted. The small degree of the possible distortion is hardly observed by current high-temperature and high-pressure x-ray techniques, and several orthorhombic and tetragonal structures have been proposed, based on in situ x-ray diffraction measurements (Kurashina et al., 2004; Ono et al., 2004; Shim et al., 2002b) or theoretical calculations (Caracas et al., 2005; Chizmeshya et al., 1996; Magyari-Köpe et al., 2002; Stixrude et al., 1996).

EoS of Ca-Pv has been determined up to CMB pressures by different groups (e.g., Kurashina et al., 2004; Mao et al., 1989;

Ono et al., 2004; Shieh et al., 2004; Shim et al., 2000a,b, 2002b; Tamai and Yagi, 1989; Wang et al., 1996). The fitting of the experimental results by third-order Birch–Murnagham EoS, yielded a unit-cell volume, $V_0 = 45.54$ Å^3, bulk modulus, K_0, ranging from 232 to 288 GPa, and its pressure derivative, K_0', within 3.9–4.5. Most of the recent results, with careful removing of the effect of deviatoric stress on the produced pressure, however, yielded the lower end values (232–236 GPa; Wang et al., 1996; Shim et al., 2000b) in this range. The results of corresponding ab initio studies (e.g., Chizmeshya et al., 1996; Karki and Crain, 1998; Stixrude et al., 1996; Wentzcovitch et al., 1995) are similar to those obtained for the experimental data. Most of these studies, both experimental and theoretical, have focused on the behavior of the cubic modification of $CaSiO_3$ under pressure.

Caracas et al. (2005) performed a detailed investigation of the major symmetry-allowed modifications of $CaSiO_3$ obtained as distortions from the parent cubic phase by means of ab initio pseudopotential theory. They examined nine modifications having different symmetries and reported that the I4/mcm phase is the most likely stable static atomic configuration up to about 165 GPa. Enthalpy difference between this I4/mcm and the cubic Pv phase increased with increasing pressure, indicating that the I4/mcm structure becomes more stable relative to the cubic structure at higher pressure. The bulk modulus was estimated to be about 250 GPa for all modifications with the exception of the R-3c structure. This theoretical K_0 is fairly similar to recent experimental values (Shim et al., 2002b; Wang et al., 1996), but much smaller than those reported in earlier nonhydrostatic experiments (Mao et al., 1989; Tamai and Yagi, 1989).

Some studies focused on the high-temperature phase change from low symmetry phase to cubic Ca-Pv. Ono et al. (2004) reported that this transition occurs at about 600–1200 K at 25–120 GPa, where the transition temperature increased with increasing pressure, consistent with the theoretical prediction (Caracas et al., 2005). These temperatures are much lower than the typical lower mantle geotherm of about 2000–2500 K, suggesting that $CaSiO_3$ may have the cubic form throughout the actual lower mantle (**Figure 7**). However, most recent ab initio molecular dynamics studies (Li et al., 2006a,b) reported very different results. They found the tetragonal phase stable even at the mantle temperatures in addition to the low-temperature stability of the orthorhombic phase. Their calculated elasticity of Ca-Pv is also very different from earlier results (Karki and Crain, 1998) particularly with respect to the shear modulus. The cause of the discrepancies is explained by Tsuchiya (2011), who advocates that even cubic Ca-Pv should have a smaller shear modulus comparable to that of tetragonal Ca-Pv.

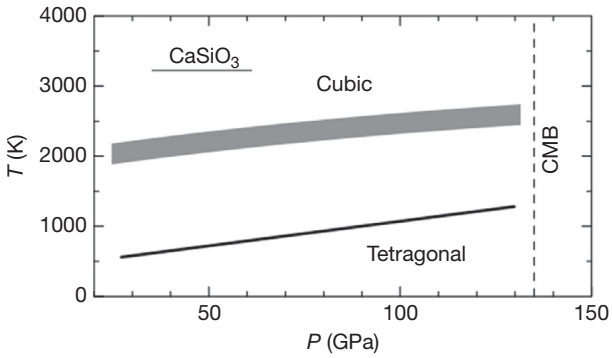

Figure 7 High P, T phase diagram for $CaSiO_3$ at lower mantle pressures summarized based on the LHDAC experiments by Kurashina et al. (2004) and Ono et al. (2004).

2.03.3.1.6 SiO_2

Recent theoretical studies suggest that a second-order displacive phase transition from stishovite (St) to the $CaCl_2$-type structure occurs at 50–60 GPa at room temperature (Kingma et al., 1995). It has also been predicted that the $CaCl_2$-type silica undergoes a further structural transition to the α-PbO_2 phase (Dubrovinsky et al., 1997; Karki et al., 1997a). The results of the experimental studies on these issues, however, have been controversial. LHDAC studies reported that the $CaCl_2$-type phase persists at least up to 120 GPa (Andrault et al., 1998), and the transition to the α-PbO_2 phase occurs at 121 GPa and 2400 K (Murakami et al., 2003). In contrast, another similar experiment showed that the α-PbO_2-like phase was formed from cristobalite above 37 GPa at room temperature, and that St directly transformed to the α-PbO_2-type structure above 64 GPa at 2500 K with a negative Clapeyron slope (Dubrovinsky et al., 2001). In addition, Sharp et al. (1999) found the α-PbO_2-type phase in a natural meteorite sample, which would have experienced very low shock pressure below 30 GPa. These discrepancies may come from various difficulties in LHDAC experiments, such as those associated with kinetic problems, temperature or pressure uncertainties, effect of different starting materials, etc.

During the last two decades, a series of theoretical studies (Dubrovinsky et al., 1997; Karki et al., 1997a; Kingma et al., 1995) also addressed this issue of the post-St phase transitions in the framework of the ab initio calculations. These early theoretical studies were limited to static conditions, the calculations being performed at $T = 0$ K, without considering the zero-point energy. To investigate the contradictory experimental results on the high-temperature phase stability of SiO_2 under high pressure, finite temperature thermal effect on the transitions obtained by these static calculations should be taken into account.

Tsuchiya et al. (2004c) predicted the high-pressure and high-temperature phase equilibrium of three ordered modifications of SiO_2 using ab initio density functional perturbation theory and the quasiharmonic approximation. The predicted St-$CaCl_2$ phase transition boundary is $P = 56 + 0.0059\,T$ (K) GPa, which is consistent with the results of a LHDAC experiment by Ono et al. (2002). This predicted slope of the St-$CaCl_2$ boundary of about 5.9 MPa K^{-1} is close to, but slightly larger than, the earlier rough estimate of 4 MPa K^{-1} (Kingma et al., 1995). The LHDAC experiment resulting in a St-α-PbO_2 boundary with a negative Clapeyron slope (Dubrovinsky et al., 2001) disagrees with the phase diagram based on Tsuchiya et al. (2004c), as shown in **Figure 8**. This disagreement may be due to experimental uncertainties and/or to kinetic problems in the former LHDAC experiment. These are supported by later calculations by Oganov et al. (2005a), though they proposed substantially lower transition pressures primarily due to the application of LDA (see **Section 2.03.2.2**).

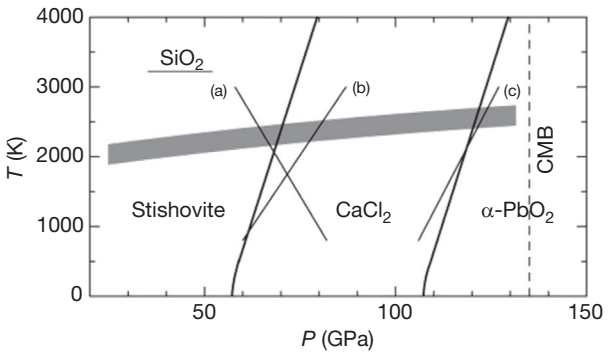

Figure 8 High P, T phase diagram for SiO_2 at lower mantle pressures predicted by the ab initio calculations by Tsuchiya et al. (2004c). The results of in situ x-ray experiments using LHDAC by (a) Dubrovinsky et al. (2001), (b) Ono et al. (2002), and (c) Murakami et al. (2003) are also shown.

On the other hand, the phase transition boundary between $CaCl_2$ and α-PbO_2 in SiO_2 is predicted to be $P = 106.3 + 0.00579\ T$ (K) GPa based on ab initio calculations (Tsuchiya et al., 2004c), which locates near the lowermost mantle P, T conditions. This calculation also indicates that the α-PbO_2-type phase is the stable form of silica at depths down to the CMB, consistent with the result of an LHDAC experiment (Murakami et al., 2003). These theoretical and experimental results also suggest that the α-PbO_2-type phase silica recently discovered in the meteorite sample might have been formed by a metastable reaction.

Irifune and Ringwood (1993) reported that St contains up to ~5% Al_2O_3 in a mid-ocean ridge basalt (MORB) composition under the uppermost lower mantle conditions. It was found that the aluminous St, containing Al_2O_3 of 4–6 wt%, transforms to a $CaCl_2$ structure at pressures of 23–25 GPa at 300 K (Bolfan-Casanova et al., 2009; Lakshtanov et al., 2007), substantially lower than those determined for pure SiO_2 St (~55–60 GPa; Ono et al., 2002; Tsuchiya et al., 2004c). Moreover, the occurrence of shear softening before the phase transition (Lakshtanov et al., 2007) and significant decreases in bulk moduli of both St and the CaCl-phase (Bolfan-Casanova et al., 2009) were observed in aluminous St. The acoustic softening associated with this transition of aluminous St in subducted oceanic crust may account for the observed localized discontinuities in the lower mantle (see the succeeding text).

2.03.3.1.7 Al-rich phase

Majorite garnet is the main host of aluminum in the mantle transition region in both pyrolite and basaltic compositions. It transforms to an assemblage of Mg-Pv + Ca-Pv at pressures corresponding to the uppermost lower mantle. Aluminum is incorporated mostly in Mg-Pv in pyrolite composition (Irifune, 1994), whereas a separate aluminous phase is formed in basaltic compositions under the P, T conditions of the lower mantle, as demonstrated by Irifune and Ringwood (1993).

The aluminous phase, named 'Al-rich phase' by these authors, was suggested to have a crystal structure similar, but not completely identical, to the calcium ferrite structure. This Al-rich phase was later proposed to have a hexagonal structure or NAL-phase (new aluminous phase; Akaogi et al., 1999; Miyajima et al., 2001; Sanehira et al., 2005), whereas others proposed that this phase possesses the calcium ferrite structure (Hirose et al., 1999; Kesson et al., 1998; Ono et al., 2005d). More recently, it was shown that both NAL-phase and the calcium ferrite phase coexist in MORB at pressures lower than ~45–50 GPa, while the former phase disappears at higher pressures (Ricolleau et al., 2008, 2010), consistent with the phase relations in the $MgAl_2O_4$–$NaAlSiO_4$ system (see the succeeding text). In any case, only very minor effects on the mineralogy and dynamics in the lower mantle are expected upon the change between these two phases under the lower mantle conditions (Sanehira et al., 2005; Shinmei et al., 2005), as the crystal structures of these phases are quite similar and yield only a slight difference in densities.

2.03.3.2 Other Minor Minerals

2.03.3.2.1 $MgAl_2O_4$, $NaAlSiO_4$

$MgAl_2O_4$ spinel is known to decompose to simple oxides of MgO and Al_2O_3 at pressure and temperatures of the mantle transition region and recombine to form a calcium ferrite ($CaFe_2O_4$, CF) type phase at about 25 GPa (Akaogi et al., 1999; Funamori et al., 1998; Irifune et al., 1991). Although the formation of an unknown phase named ε-phase (Liu, 1978) was reported at a similar pressure at 1300 K in LHDAC experiments, none of the subsequent LHDAC and KMA experiments using both quench and in situ x-ray measurements have confirmed this phase. Instead, it has been shown that the CF-phase further transforms to a calcium titanate ($CaTiO_4$, CT) phase at pressures of ~40–45 GPa (Funamori et al., 1998). An ab initio periodic linear combination of atomic orbitals calculation by Catti (2001) demonstrated that the calcium titanate structure is stable relative to the calcium ferrite structure at pressures greater than ~39–57 GPa, but this phase change was not confirmed by a recent pseudo-potential study (Tsuchiya, 2011).

$NaAlSiO_4$ also adopts the calcium ferrite structure at pressures above 25 GPa (Akaogi et al., 1999; Liu, 1977), although the formation of the complete solid solutions between this and $MgAl_2O_4$ was not reported, as there is a region of the hexagonal phase (NAL-phase) in the intermediate region of these end-member compositions (Akaogi et al., 1999; Ono et al., 2009; Shinmei et al., 2005). It was demonstrated that the CF-type $NaAlSiO_4$ is stable at least at pressures up to 75 GPa and temperatures to 2500 K on the basis of LHDAC experiments (Tutti et al., 2000).

More recently, the stability relations of the CF phase and the hexagonal phase in the joint $NaAlSiO_4$–$MgAl_2O_4$ were investigated both experimentally and theoretically (Imada et al., 2011; Kawai and Tsuchiya, 2012). The study demonstrated that the hexagonal phase is no more stable at pressures higher than ~45 GPa and completely transforms to the CF phase. Kawai and Tsuchiya (2012) also showed that the NAL–CF transition would not cause any notable velocity changes in the lower mantle.

2.03.3.2.2 $KAlSi_3O_8$, $NaAlSi_3O_8$

$KAlSi_3O_8$-rich feldspar, an important mineral in K-rich basalt (e.g., Wang and Takahashi, 1999) and continental crust

and marine sediment lithologies (Irifune et al., 1994), transforms to the hollandite structure via a mixture of $K_2Si_2O_5$ wadite + Al_2O_5 kyantite + SiO_2 coesite at about 9 GPa. $KAlSi_3O_8$ hollandite plays an important role in fractionation of some trace elements because of its peculiar tunnel structure that accommodates large ion lithophile elements (Irifune et al., 1994; Rapp et al., 2008). Although a LHDAC study suggested that this structure is stable almost throughout the lower mantle *P*, *T* conditions (Tutti et al., 2001), recent in situ x-ray diffraction studies using DAC with a helium pressure medium at room temperature (Ferroir et al., 2006) and KMA at high pressure and high temperature demonstrated that the hollandite transforms to an unquenchable phase, named 'hollandite II' (Sueda et al., 2004), at about 22 GPa at room temperature with a positive Clapeyron slope. Although only a slight modification in crystal structures between these phases was noted (Ferroir et al., 2006), this transition may significantly affect partitioning of some trace elements between the K-hollandite and coexisting melts in the lower mantle.

Ab initio calculations (Caracas and Boffa Ballaran, 2010; Kawai and Tsuchiya, 2013; Mookherjee and Steinle-Neumann, 2009) demonstrated that the transition of K-hollandite to the holandite II structure is associated with an elastic instability as suggested by Hirao et al. (2008). Kawai and Tsuchiya (2013) further indicated clearly that the transition has the second-order nature. These studies also showed that the hollandite-II phase remains stable up to the CMB condition.

$NaAlSi_3O_8$-rich hollandite was found in shock veins of some meteorites (e.g., Gillet et al., 2000; Tomioka et al., 2000). However, attempts to reproduce the hollandite with such compositions by high-pressure experiments have failed (Liu, 2006; Yagi et al., 1994), as the solubility of this component is limited to about 50 mol% at pressures of ~22 GPa and at temperatures up to 2500 K. Thus, this phase could have been formed metastably in a very short period of time under shock compression in the parental bodies of these meteorites. A recent ab initio computation supports this idea, showing that $NaAlSi_3O_8$-rich hollandite is unstable relative to other possible phase assemblages at pressures at least to 40 GPa (Deng et al., 2010).

2.03.3.2.3 CAS phase

The 'CAS (Ca- and Al-rich silicate) phase' was first described by Irifune et al. (1994) as a new Ca- and Al-rich high-pressure phase in a continental crust composition at pressures above ~15 GPa and was suggested to be a major host for aluminum and calcium in the subducted marine sediments in the mantle transition region. Subsequent experimental studies demonstrated that this phase has the ideal composition of $CaAl_4Si_2O_{11}$, possessing a hexagonal barium ferrite-type structure with space group $P6_3/mmc$ (Gautron et al., 1999). Moreover, this high-pressure phase with a composition of $(Ca_xNa_{1-x})Al_{3+x}Si_{3-x}O_{11}$ was recently discovered in a Shergottite shocked Martian meteorite in association with St and/or K,Na-rich hollandite (Beck et al., 2004), both of which are known to be stable only at pressures above ~9 GPa.

The CAS phase is suggested to have silicon in fivefold coordination in a trigonal bipyramid site at high pressure and high temperature and is supposed to decompose into fourfold and sixfold coordinations upon quenching and subsequent release of pressure (Gautron et al., 1999). In situ Raman spectroscopy and x-ray diffraction measurements actually indicated the formation of fivefold coordinated silicon under pressure, which should play an important role in the transport properties of minerals through the formation of oxygen vacancies (Gautron et al., 2005).

Stability of the CAS phase was determined based on high-pressure experiments at pressures to 23 GPa and temperatures to 2073 K, combined with thermodynamic analyses, showing that this phase is stable above ~12 GPa and at temperatures exceeding 1373 K (Akaogi et al., 2009). The low-pressure phase assemblage is reported as garnet + kyanite + corundum, while an assemblage of garnet + St + corundum is stable at the lower temperatures. It has also been reported that grossular garnet decomposes to Ca-Pv + the CAS phase at pressures above 20 GPa and temperatures higher than ~1400 K (Greaux et al., 2011).

2.03.3.2.4 Phase D, δ-AlOOH

Phase D was first noted by Liu (1986) as a new dense hydrous magnesium silicate (DHMS) phase in serpentine and was later confirmed by in situ x-ray diffraction (Irifune et al., 1996b). Both the x-ray power diffraction profile and the chemical composition of this phase were also refined on the quenched sample (Irifune et al., 1996b; Kuroda and Irifune, 1998). Two groups subsequently succeeded in refining its crystal structure independently (Kudoh et al., 1997; Yang et al., 1997). The stability of phase D has since been studied experimentally using both KMA (Frost and Fei, 1998; Irifune et al., 1998b; Ohtani et al., 1997) and LHDAC (Shieh et al., 1998). This demonstrated that this phase has a wide stability field up to 4050 GPa at temperatures to ~1800 K, whereas it dehydrates to form an assembly containing Mg-Pv and Mw at higher temperatures (Shieh et al., 1998).

Serpentine is the major hydrous mineral in the subducted slab, and phase D should be the only possible DHMS present in the upper part of the lower mantle transported via the subduction of slabs (Irifune et al., 1998b; Ohtani et al., 2004; Shieh et al., 1998), although the newly found δ-AlOOH (Suzuki et al., 2000) could be an alternative water reservoir in the lower mantle if a certain amount of water is retained in the crustal components in the subducted slabs. δ-AlOOH was both experimentally and theoretically (Sano et al., 2008; Tsuchiya and Tsuchiya, 2011a) reported to be stable under almost the entire *P*, *T* conditions of the lower mantle. The extraordinarily high stability of δ-AlOOH as a hydrous phase suggests that this phase could be a potentially important water carrier into the core. δ-AlOOH is predicted to eventually transform to a pyrite-type structure at ~150 GPa before its dehydration (Tsuchiya and Tsuchiya, 2011a). δ-AlOOH is also important in the context of the hydration of St because of the similarity in their crystal structures (Panero and Stixrude, 2004). Incorporation of the AlOOH component into St might significantly affect the post-St transition pressure (Lakshtanov et al., 2007).

For both phase D and δ-AlOOH, structural changes associated with hydrogen bond symmetrization are expected to occur on the basis of ab initio calculations (Tsuchiya et al., 2002, 2005a), which should affect the compressional behavior and, hence, density changes of these hydrous phases in the lower mantle. Tsuchiya (2013) recently predicted that phase

D transforms to an assemblage of St plus a new hydrous phase $MgSiO_4H_2$ with monoclinic symmetry in a limited pressure range between 40 and 52 GPa, based on ab initio calculations. This phase may form solid solutions with AlOOH, and should be further explored to identify the plausible hydrous phases in the lower mantle.

2.03.3.2.5 $MgCO_3$, $CaCO_3$

Carbonates are important constituents of pelagic sediments, parts of which are supposed to subduct into the mantle. It has been shown that $MgCO_3$ magnesite is the major carbonate in the mantle (e.g., Biellmann et al., 1993), and its stability under high pressure has been studied using LHDAC. Magnesite was reported to be stable at pressures up to 80 GPa almost throughout the lower mantle (Fiquet et al., 2002; Gillet, 1993), but a recent in situ x-ray diffraction study demonstrated it transforms to an unknown phase (magnesite II) at pressures above ~115 GPa, at 2000–3000 K (Isshiki et al., 2004). Although the dissociation of magnesite into assemblages of $MgO + CO_2$ (Fiquet et al., 2002) or $MgO + C + O_2$ (Liu, 1999) was suggested on the basis of thermodynamic considerations, such reactions are unlikely to occur along appropriate geotherms in the lower mantle (Isshiki et al., 2004; Oganov et al., 2008). Oganov et al. (2008) also predicted the formation of other high-pressure forms of $MgCO_3$ in the lowermost part of the mantle, which are different from the magnesite II reported by Isshiki et al. (2004). Accordingly, the stable structure of $MgCO_3$ in this region of the mantle remains an open question.

In contrast, certain amounts of $CaCO_3$ could survive in the subducted slabs without decarbonation or reaction with surrounding minerals, due to the low temperatures of the slabs, and thus are delivered into the lower mantle. $CaCO_3$ adopts the aragonite structure under P, T conditions of the uppermost mantle, and this was found to transform to a high pressure form with an orthorhombic symmetry at pressures greater than ~40 GPa and at temperatures 1500–2500 K using LHDAC (post-aragonite phase; Ono et al., 2005c). Although the possibility of the transformation of $CaCO_3$ aragonite to a trigonal phase is suggested on the basis of DAC experiments at room temperature (Santillán and Williams, 2004), this phase was demonstrated to have been metastably formed and the transformation of the post-aragonite phase into an orthopyroxene-type structure (post-postaragonite phase) was confirmed at pressures above ~130 GPa and temperatures above ~1500 K by in situ x-ray observations (Ono et al., 2007), as predicted by an ab initio study (Oganov et al., 2006). Thus, $MgCO_3$ and possibly $CaCO_3$ are the potential hosts of CO_2 throughout most parts of the lower mantle, except for the bottom parts of the D″ layer (Isshiki et al., 2004; Oganov et al., 2008).

2.03.4 Phase Transitions and Density Changes in Mantle and Slab Materials

2.03.4.1 Chemical Compositions and Density Calculations

Subducting oceanic lithosphere is modeled by layers of basaltic oceanic crust of ~6 km thickness, underlain by thicker layers (~50–100 km) of residual harzburgite and fertile lherzolite, which are covered with thin (~1 km) terrigeneous and/or pelagic sediments. Typical chemical compositions of these lithologies are listed in **Table 1**. Most parts of the sedimentary materials are believed to be trapped to form accretion terrains underneath island arcs upon subduction of slabs at ocean trenches, although geochemical evidence suggests certain parts of such materials may be subducted deeper into the mantle (e.g., Loubet et al., 1988). At least part of the bottom warmer lherzolite layer of a slab may also be assimilated to the surrounding mantle during subduction in the upper mantle and mantle transition region, and thus the slab approaching the 660 km seismic discontinuity can reasonably be modeled by a layered structure of basaltic and harzburgitic rocks (Ringwood and Irifune, 1988).

The chemical composition of the lower mantle has been a major controversial issue in the mineralogy of the Earth's interior. Some (e.g., Ringwood, 1962) believe peridotitic or pyrolitic materials are dominant in the whole mantle, while others (e.g., Anderson, 1989; Hart and Zindler, 1986; Liu, 1982) claim more Si-rich chondritic materials should be representative for the composition of the lower mantle (**Table 1**). The difference is based on rather philosophical arguments on the origin and subsequent differentiation processes of the Earth, which are critically dependent on the models of condensation/evaporation processes of elements and compounds in the primordial solar system and the possible formation of a deep magma ocean in the early stage of the formation of the Earth. As the elastic properties, particularly those related to

Table 1 Representative chemical compositions of lower mantle and those related to subducting slabs

	Lower mantle				
	Chondrite	*Pyrolite*	*Harzburgite*	*MORB*	*Continental crust*
SiO_2	53.8	44.5	43.6	50.4	66.0
TiO_2	0.2	0.2	–	0.6	0.5
Al_2O_3	3.8	4.3	0.7	16.1	15.2
Cr_2O_3	0.4	0.4	0.5	–	–
FeO	3.5	8.6	7.8	7.7	4.5
MgO	35.1	38.0	46.4	10.5	2.2
CaO	2.8	3.5	0.5	13.1	4.2
Na_2O	0.3	0.4	–	1.9	3.9
K_2O	–	0.1	–	0.1	3.4

Chondrite, Liu (1982); pyrolite, Sun (1982); harzburgite, Michael and Bonatti (1985); MORB, Green et al. (1979); continental crust, Taylor and McLennan (1985).

shear moduli, of high-pressure phases have not been well documented under the pressure and temperature conditions of the lower mantle, it is hard to unambiguously evaluate the feasibility of these two alternative composition models in the light of mineral physics and seismological observations (e.g., Bina, 2003; Mattern et al., 2005). Some efforts have been made to directly measure the elastic properties under the *P*, *T* conditions of the lower mantle (Murakami et al., 2012), but we need further data on the elastic properties of major minerals in the lower mantle and their pressure, temperature, and compositional dependencies to reach a decisive conclusion on the feasible chemical composition. Moreover, the knowledge of variation of temperature with depth is vital to address this issue, but this also has not been well constrained in the lower mantle.

Here, we assume the whole mantle is of a pyrolitic composition to address the phase transitions and associated density changes in the lower mantle, as there are significant chemical variations in the chondritic models and also because high-pressure experimental data on these compositions have been scarce to date. We also assume the major lithologies transported into the lower mantle via subduction of slabs are of MORB and harzburgite compositions. Some recent studies suggest that the continental crust may also be delivered to the mantle transition region (Ichikawa et al., 2013; Kawai et al., 2013), but it should be difficult to subduct further into the lower mantle, considering the density relations between the continental crust material and surrounding mantle at around the 660 km discontinuity (Irifune et al., 1994; Ishii et al., 2012; Kawai et al., 2013). Phase transitions in MORB have been extensively studied down to the depths near the mantle–core boundary. In contrast, although virtually no experimental data exist on harzburgite compositions in this depth region, they can be reasonably estimated from those available on the high-pressure phases with simple chemical compositions, as harzburgitic compositions have a minor amount of Fe and only very small amounts of Ca, and Al, and are well approximated by the MgO (FeO)–SiO_2 system.

We calculated the density changes in pyrolite, harzburgite, and MORB compositions using available experimental data as follows: The densities of the individual high-pressure phases appeared in these lithologies were calculated at given pressures using the thermal EoS combining third-order Birch–Murnaghan EoS and Debye theory along an appropriate geotherm, using the PVT-EoS parameters given in Table 2. The resultant density changes of individual phases along the geotherm are depicted in Figure 9. The density changes in the bulk rocks were then calculated using the proportions of the individual phases with pressure along the geotherm.

Although some recent studies suggest that sub-adiabatic temperature gradients are required to match the observed and calculated density and bulk sound velocity for pyrolitic compositions (Bina, 2003; Mattern et al., 2005), we simply assumed adiabatic temperature changes throughout the lower mantle (i.e., 1900 K at 660 km and 2450 K at 2890 km with an averaged gradient of $dT/dz = \sim 0.3$ K km^{-1}; e.g., Brown and Shankland, 1981) as such conclusions are not robust, given the uncertainties in both mineral physics measurements and seismological observations. In addition, significantly sharp temperature increases are expected to occur near the mantle–core boundary and presumably near the 660 km discontinuity as these regions are accompanied by chemical changes and form thermal boundary layers, which are also not taken into account in the present calculations.

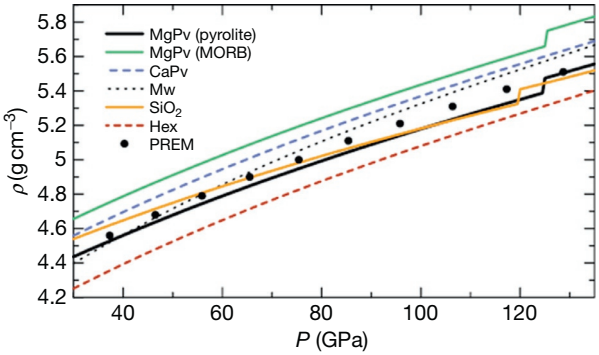

Figure 9 Density changes in major minerals constituting pyrolite and mid-ocean ridge basalt (MORB) compositions as a function of pressure along the adiabatic geotherm, calculated with EoS using the mineral physics parameters listed in Table 2. The density changes of Mg-Pv and Mw in the harzburgite composition are very close to, but slightly lower than, those of the corresponding phases in pyrolite, which are not shown in this figure. Dots represent the densities in PREM. Hex, hexagonal aluminous phase.

Table 2 PVT-EoS parameters of lower mantle phases determined from various experimental and theoretical data and their systematics

	Mg-Pv	*Fe-Pv*	*Al_2O_3-Pv*	*Mg-PPv*	*Ca-Pv*	*MgO*	*FeO*	*SiO_2-St*	*SiO_2-α-PbO_2*
V_0 (cm^3 mol^{-1})	24.45	25.48	24.77	24.6	27.45	11.36	12.06	14.02	13.81
B_0 (GPa)	257	281	232	226	236	158	152	314	325
B'	4.02	4.02	4.3	4.41	3.9	4.4	4.9	4.4	4.2
Θ_D (K)	1054	854	1020	1040	984	725	455	1044	1044
γ	1.48	1.48	1.48	1.55	1.53	1.5	1.28	1.34	1.34
q	1.2	1.2	1.2	1.2	1.6	1.5	1.5	2.4	2.4

Mg-Pv (Fiquet et al., 2000; Shim and Duffy, 2000; Sinogeikin et al., 2004; Tsuchiya et al., 2004a, 2005b), Fe-Pv (Jeanloz and Thompson, 1983; Kiefer et al., 2002; Mao et al., 1991; Parise et al., 1990), Al_2O_3-Pv (Thomson et al., 1996; Tsuchiya et al., 2005c), Mg-PPv (Tsuchiya et al., 2004a, 2005b), Ca-Pv (Karki and Crain, 1998; Shim et al., 2000b; Wang et al., 1996), MgO (Fiquet et al., 1999; Sinogeikin and Bass, 2000), FeO (Jackson et al., 1990; Jacobsen et al., 2002; Systematics), SiO_2 (Andrault et al., 2003; Karki et al., 1997a; Ross et al., 1990; Tsuchiya et al., 2004c).

The high-T Birch–Murnaghan equation was applied only for the hexagonal aluminous phase with parameters: $V_0 = 110.07$ cm^3 mol^{-1}, $B_0 = 185.5$ GPa, $B' = 4$ (fix), $dB/dT = -0.016$ GPa K^{-1}, and $\alpha_0 = 3.44 \times 10^{-5}$ K^{-1} (Shinmei et al., 2005; Sanehira et al., 2005).

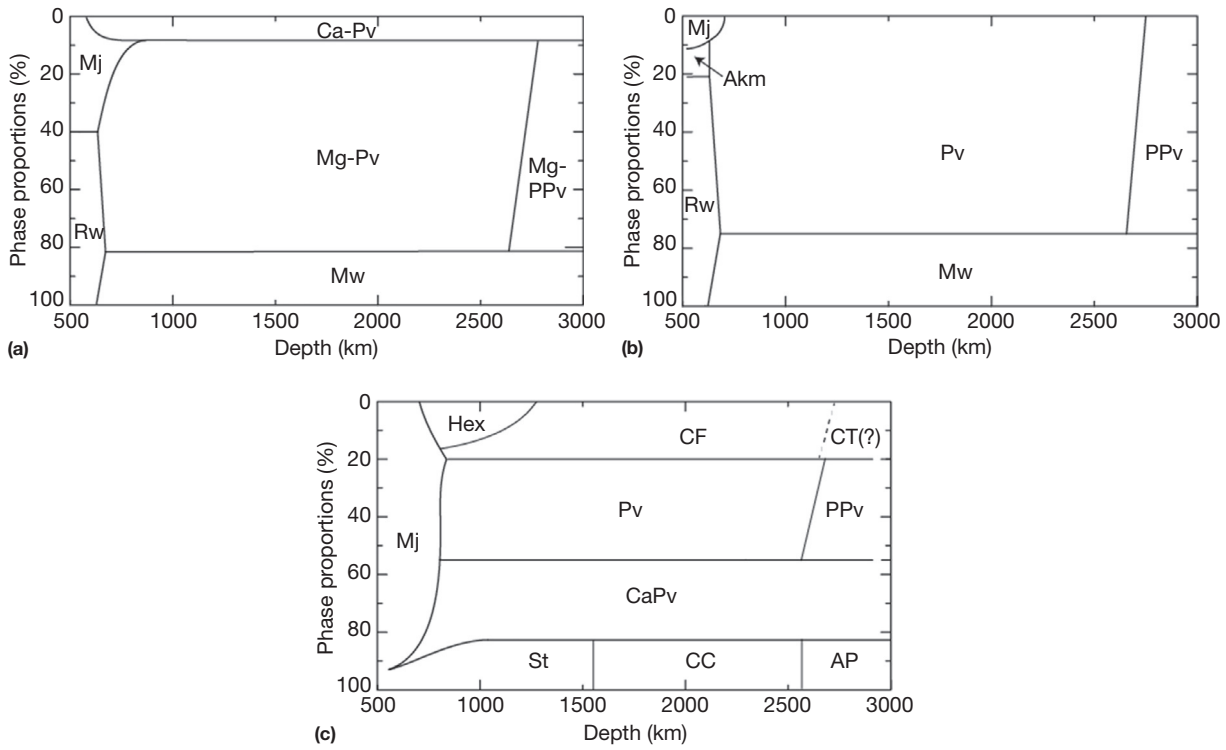

Figure 10 Mineral proportion changes in pyrolite (a), harzburgite (b), and MORB (c) as a function of depth along the adiabatic geotherm. Akm, akimotoite; Rw, ringwoodite; CF, calcium-ferrite phase; CT, calcium-titanite phase; CC, $CaCl_2$ phase; AP, α-PbO_2 phase. Data taken from Irifune and Ringwood (1987, 1993), Irifune (1994), Hirose et al. (1999, 2005), Murakami et al. (2004a, 2005), Ono et al. (2001, 2005d), Irifune et al. (2010), and Ricolleau et al. (2010).

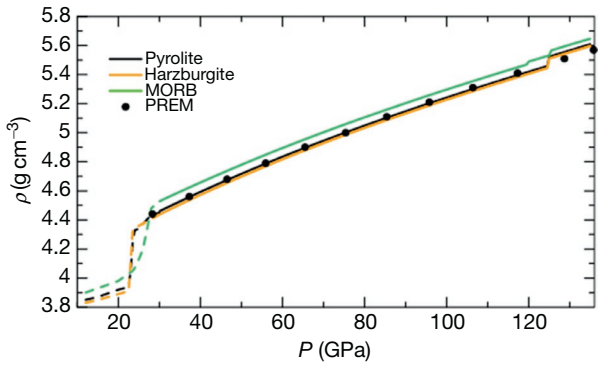

Figure 11 Bulk density variations of pyrolite, harzburgite, and MORB calculated based on the PVT-EoS of constituent mineral phases (**Table 1** and **Figure 9**) and their proportions (**Figure 10**). Broken lines at pressures lower than 30 GPa are results in Irifune (1993).

The mineral proportion changes in pyrolite, harzburgite, and MORB compositions are shown in **Figure 10**, while the calculated density changes of these lithologies are depicted in **Figure 11**. The density changes at pressures lower than 30 GPa are based on an earlier estimate of Irifune (1993), using a similar method and mineral physics parameters. Although the density change in pyrolite seems to agree well with that of PREM (Preliminary Reference Earth Model; Dziewonski and Anderson, 1981), the latter estimate inevitably has significant uncertainties, as this density profile is rather indirectly determined from seismic velocities with some assumptions. The calculated density values may also have significant errors, mainly due to the uncertainty in the geotherm stated in the above. Nevertheless, mineral physics parameters to constrain the density have been reasonably well determined, mostly on the basis of in situ x-ray diffraction measurements, and the differences among these calculated density profiles are regarded as robust results.

2.03.4.2 Phase and Density Relations

2.03.4.2.1 Pyrolite

Figure 10(a) illustrates the phase transitions in pyrolite as a function of depth. Pyrolite transforms from an assemblage of ringwoodite (Rw) + majorite garnet (Mj) + Ca-Pv under the P, T conditions of the mantle transition region to that of Mg-Pv + Ca-Pv + Mj + Mw at depths near the 660 km seismic discontinuity. The spinel to postspinel transition in this composition is actually believed to have occured at pressures near 23.5 GPa and at a temperature of ~2000 K, on the basis of quench experiments (e.g., Irifune, 1994). The slope of this phase transition boundary has also been determined by both quench experiments (Ito and Takahashi, 1989) and calorimetric measurements (Akaogi and Ito, 1993), yielding a value of ~ -3 MPa K^{-1}. Although some recent studies suggest somewhat lower transition pressures (Fei et al., 2004; Irifune et al., 1998a,b; Katsura et al., 2003; Kono et al., 2010; Tange et al., 2009a) and larger Clapeyron slope (Fei et al., 2004; Katsura

et al., 2003), the spinel to postspinel transition is generally believed to be the main cause of the 660 km discontinuity, which is followed by the smeared out transition of majorite to Pv over a pressure interval of ~2 GPa (Irifune, 1994; Nishiyama et al., 2004).

Mg-Pv is stable throughout most regions of the lower mantle, but it is found to transform to the Mg-PPv with the $CaIrO_3$ structure in a peridotite composition at pressures close to those near the top of the D″ layer. A small density jump of about 1–1.5% is expected to occur associated with this transition in the lower mantle. Ca-Pv, on the other hand, is likely to adopt the cubic structure throughout the lower mantle. On the other hand, Mw remains in the rock salt (B1) structure at pressures to ~80 GPa, where it may transform to the NiAs (B8) structure if iron concentration is very high (Fei and Mao, 1994). A high-spin to low-spin transition has also been demonstrated to occur in this phase over the pressure range of the upper to middle lower mantle, as shown in Figure 6, which may yield an additional gradual density increase over this interval and also affect partitioning of iron between this phase and the ferro-silicate Pv (Irifune et al., 2010).

Although element partition data among the coexisting phases under the lower mantle conditions have been limited to those below ~50 GPa in KMA for the pyrolite composition (e.g., Irifune, 1994; Irifune et al., 2010; Wood, 2000), some results have also been obtained using LHDAC combined with ATEM at higher pressures (e.g., Murakami et al., 2005; Ono et al., 2005d; Sinmyo and Hirose, 2013). These studies, particularly those using KMA, demonstrated that the presence of a minor amount (~5 wt%) of Al_2O_3 in Mg-Pv has dramatic effects on the partitioning of iron between Mg-Pv and Mw, in addition to those on the compressibility of Mg-Pv, below ~30 GPa. Nevertheless, the variations in iron partitioning between the two phases would not cause any significant changes in the bulk density of the pyrolitic mantle (e.g., Bina, 2003; Irifune et al., 2010). Some notable changes in the iron partitioning between Mg-Pv and Mw have also been suggested upon the Pv–PPv transition in a recent LHDAC study (Murakami et al., 2005; Sinmyo et al., 2011), but it may also yield invisible effects on the density change in the pyrolite bulk composition.

2.03.4.2.2 Harzburgite

Harzburgite, with Mg# (=Mg/(Mg+Fe)×100)=~92 as listed in Table 1, crystallizes to form an assemblage of ~80% olivine and ~20% orthopyroxene at depths in the uppermost mantle, which transforms to Mg-Pv and Mw near the 660 km discontinuity via an assemblage of Rw+Mj+akimotite (Akm, ilmenite form of $MgSiO_3$) as shown by Irifune and Ringwood (1987). Although no experimental data have been available at pressures higher than 26 GPa, the nature of the phase transition in this composition can be evaluated based on the changes in these two phases under the lower mantle conditions. The result estimated along the adiabatic geotherm is shown in Figure 10(b), which shows that this lithology is less dense than pyrolite throughout the lower mantle except for a very limited region immediately below the 660 km discontinuity (Irifune and Ringwood, 1987), where the density relation reverses due to the completion of the spinel to postspinel transition at lower pressures in the harzburgite composition.

It was suggested that Fe significantly lowers the Pv–PPv transition pressure (Mao et al., 2004, 2005), while more recent studies showed that the effect of iron on this transition pressure is rather opposite (Andrault et al., 2010; Hirose et al., 2008; Sinmyo et al., 2008) as stated earlier. On the other hand, the presence of Al may also slightly affect this transition pressure (Tateno et al., 2005; Tsuchiya and Tsuchiya, 2008; Tsuchiya et al., 2005c), as shown in Figures 2–4. In harzburgite compositions, Mg-Pv should have less alumina and iron content as compared with those of Mg-Pv in pyrolite under the lower mantle conditions. However, as the differences in the contents of Fe and Al between these two lithologies are relatively small, we assume the Pv–PPv transition occurs at the same pressure in these compositions, although further detailed experimental studies on these compositions are needed to resolve this issue.

2.03.4.2.3 Mid-ocean ridge basalt

Phase transitions in basaltic compositions, such as illustrated in Figure 10(c) for a MORB composition, are quite different from those expected in pyrolite and harzburgite compositions. Basaltic compositions are shown to crystallize to Mj+small amounts of St in the mantle transition region (Hirose et al., 1999; Irifune and Ringwood, 1987, 1993; Ono et al., 2001), and then progressively transform to an assemblage of Ca-Pv+Mg-Pv+St+Al-rich phase (NAL phase, which is replaced by the CF phase at pressures greater than ~50 GPa according to Ricolleau et al., 2010) over a wide pressure range of ~3 GPa (from ~24 to ~27 GPa). Although the garnetite facies of MORB, composed mainly of Mj, are substantially denser than pyrolite, a density crossover is expected to occur in a limited depth range (660 to ~720 km) of the uppermost lower mantle due to this smeared-out nature of the garnetite to Pv transition in MORB.

Once Ca-Pv and Mg-Pv are formed in basaltic compositions, it is shown that they become denser than pyrolite or peridotite throughout almost the entire region of the lower mantle (Hirose et al., 1999, 2005; Irifune and Ringwood, 1993; Ono et al., 2001, 2005d). As St is highly incompressable (Figure 9), the density of the perovskite facies of basaltic compositions may approach that of the pyrolitic composition with increasing pressure. However, the transition of St to $CaCl_2$ (CC) and α-PbO_2 (AP) structures should keep this lithology denser than pyrolite throughout the lower mantle, as shown in Figure 11. In fact, most recent experimental studies using LHDAC (Hirose et al., 2005; Ono et al., 2005d; Ricolleau et al., 2010) conclude that densities of basaltic compositions are higher than those in the representative model mantle compositions throughout the lower mantle by about 0.02–0.08 g cm^{-3}, depending on the adopted pressure scale for gold.

2.03.5 Mineralogy of the Lower Mantle

2.03.5.1 The 660 km Discontinuity

The 660 km seismic discontinuity is a globally recognized feature, and is the sharpest among the proposed discontinuities throughout the whole mantle. The cause of this discontinuity (chemical or phase transition boundary) has been a major controversial issue in Earth sciences as stated

earlier, but the detailed experimental study based on quench experiments using KMA strongly suggested that this is caused by the spinel to postspinel transition in a pyrolite or peridotitic mantle (Irifune, 1994; Ito and Takahashi, 1989). The experimental data on the sharpness, pressure, and Clapeyron slope of this phase transition all seemed to be consistent with those estimated from seismological observations.

However, recent experimental, seismological, and geodynamic studies cast some doubt on the simple idea of the phase transition. Precise in situ x-ray diffraction measurements using KMA demonstrated that this transition occur at pressures somewhat (~2.5–1 GPa) lower than that corresponding to the 660 km discontinuity (Fei et al., 2004; Irifune et al., 1998a; Katsura et al., 2003; Matsui and Nishiyama, 2002; Nishiyama et al., 2004), although some LHDAC experiments reported the phase transition pressure is rather consistent with that of the discontinuity (Chudinovskikh and Boehler, 2001; Shim et al., 2001a). Meanwhile, reevaluation of the transition pressure using the latest MgO pressure scales based on a theoretical analysis (Tange et al., 2009a) and sound velocity measurement (Kono et al., 2010) shows that the pressure for the spinel to postspinel transition is close to, but slightly (~0.5–1 GPa) lower than, that of the 660 km discontinuity. In addition, seismological observations suggest this discontinuity is divided into several discontinuities in some areas (e.g., Simmons and Gurrola, 2000), which cannot be explained by the spinel to postspinel transition alone.

Moreover, recent in situ x-ray diffraction measurements have suggested that the Clapeyron slope of the spinel to postspinel transition is significantly larger (-2 to -0.4 MPa K^{-1}; Fei et al., 2004; Katsura et al., 2003; Litasov et al., 2005) than previously thought (~-3 MPa K^{-1}; Akaogi and Ito, 1993; Ito and Takahashi, 1989) and ab initio prediction (~-2 MPa K^{-1}; Yu et al., 2006). If this is the case, it should be difficult to trap the subducted slabs underneath many subduction zones near this boundary, known as 'stagnant slabs' (e.g., Fukao et al., 1992, 2001; Zhao, 2004), in the light of geodynamics calculations (e.g., Davis, 1998), unless a large viscosity jump at the 660 km depth and a concept of trench retreat are introduced (Torii and Yoshioka, 2007). Furthermore, the observed depth variations of the 660 km discontinuity sometimes reach ~30–40 km (e.g., Flanagan and Shearer, 1998), which corresponds to a temperature difference of ~1000 K if we adopt $dP/dT = -1$ MPa K^{-1} for the spinel–postspinel transition boundary. Such a temperature difference between subducting slabs and the surrounding mantle near the 660 km discontinuity should be too large to be accounted for by seismological tomographic observations or by any reasonable models of thermal structures of the subducting slabs.

Nevertheless, considering the uncertainties in pressure and temperature measurements in the in situ x-ray observations in KMA due to unresolved problems on the pressure scales and temperature measurements at high pressure using thermocouple electromotive force, it is generally accepted that the 660 km discontinuity can be explained by the spinel–postspinel transition in a pyrolitic mantle. Recent studies also suggested possibilities of elucidating the multiple nature and the depth variation of the 660 km discontinuity by reactions involving akimotite at relatively low temperatures (Hirose, 2002; Weidner and Wang, 2000; Zhou et al., 2013). In this case, the high velocity/density gradients shown in some representative seismological models at depths of 660–750 km may be largely explained by the smeared-out transition of majorite to perovskite in pyrolite over this depth interval (Irifune, 1994).

Models with chemical composition changes may reconcile the contradictory experimental and seismological observations regarding the 660 km discontinuity. If the spinel to postspinel transition does occur at pressures lower than that of 660 km (~23.5 GPa) by, for instance, 1 GPa, the phase discontinuity should locate at about 630 km in a pyrolite mantle. As the oceanic crust component of the subducted slab, modeled by the MORB composition, becomes less dense than the surrounding pyrolite mantle immediately below this depth as shown in **Figure 11**, it should have been buoyantly trapped on this primordial '630 km discontinuity' at the initial stage of the onset of operation of plate tectonics.

The delamination and accumulation of the former oceanic crust, transformed to garnetite in the mantle transition region, can be enhanced by its plausible different viscosity relative to the surrounding mantle (Karato, 1997) and extremely slow reaction kinetics upon transitions to the denser phase assemblages including Mg-Pv (Kubo et al., 2002) or majorite (Nishi et al., 2011). Continuation of this process of trapping basaltic crust over a couple of billion years should yield a thick (on average ~50–100 km, depending on the production rates of oceanic crust and efficiency of the trapping) layer of garnetite near the 630 km discontinuity. The garnetite layer develops both upward and downward from this primordial discontinuity if it isostatically floats on this boundary. The bottom of this garnetite layer eventually reaches 660 km, under which the harzburgite portion of the subducted slab should be present. In fact, some mineral physics studies suggest the uppermost lower mantle can be Mg-rich as compared with the deeper regions (Bina, 2003; Nakagawa et al., 2010).

Accumulation of oceanic crust above the 660 km seismic discontinuity was originally proposed by Anderson (1979) to form an eclogite layer in the lower half of the upper mantle and throughout the mantle transition region. He later confined it to the latter region and favored a more mafic lithology named 'piclogite' (e.g., Anderson and Bass, 1986; Duffy and Anderson, 1989). Ringwood (1994) also proposed the presence of a thin (~<50 km) layer of former basaltic crust immediately above the lower mantle, as a result of accumulation of relatively young and warm slab materials at the 660 km discontinuity. The above model of a thicker garnetite layer is thus in between those proposed by these authors. Some numerical analyses with seismological data (Camarano et al., 2009) and geodynamic modeling (Nakagawa et al., 2010) using available mineral physics data also suggest that the proportion of MORB would increase with depth in the mantle transition region.

On the other hand, recent developments in combined in situ x-ray and ultrasonic interferometry measurements in KMA allowed us to precisely determine sound velocities of high-pressure minerals under the pressure and temperature conditions of the mantle transition region (Higo et al., 2008; Li, 2003). The results using this technique demonstrated that both pyrolite and MORB compositions fail to explain the seismological velocity models for the lower parts of the mantle transition region (Irifune et al., 2008; Kono et al., 2012), consistent with the results of ab initio calculations (Tsuchiya,

2011). Irifune et al. (2008) suggested that the bottom parts of the mantle transition region may be filled with harzburgite instead of MORB, as discussed above, and may be the main body of the subducted slabs. Further studies are needed to identify the chemical composition of this region of the mantle around 660 km, which is important in addressing the nature and origin of this largest seismic discontinuity in the mantle.

2.03.5.2 Middle Parts of the Lower Mantle

The uppermost part of the lower mantle is believed to be structurally and chemically heterogeneous due to the presence of stagnant slabs (Fukao et al., 1992, 2001; Zhao, 2004) which were originally proposed as 'megaliths' on the basis of high-pressure experimental studies (Ringwood, 1994; Ringwood and Irifune, 1988). Moreover, there are some areas where slabs appear, from tomographic images, to penetrate deep into the lower mantle (e.g., Fukao et al., 2001; van der Hilst et al., 1997), which should contribute to the observed reflection, refraction, or conversion of seismic waves at these depths. Thus, the presence of subducted slabs in the uppermost lower mantle may, at least partly, contribute to the transitional nature of the seismic velocities for a depth interval between 660 and ~750 km in some global models of the velocity profiles.

In the deeper parts of the lower mantle, discontinuous changes in seismic velocities have also been suggested to occur, particularly at depths 900–1200 km beneath some subduction areas (Kaneshima, 2003; Kawakatsu and Niu, 1994; Kruger et al., 2001; Niu and Kawakatsu, 1996). As there are no major phase transitions in the mantle material modeled by pyrolite as shown in **Figure 10(a)**, such discontinuous changes are most likely to be related to the subducted slab materials. Both basaltic and underlying harzburgite layers of such slabs may yield locally high acoustic impedance to produce seismic discontinuities, because these basaltic and harzburgite materials seem to have seismic velocities higher than those of the mantle material in this region of the lower mantle (e.g., Bina, 2003), in addition to their lower temperatures compared to the surrounding mantle.

In further deeper parts of the lower mantle (~1200–1850 km in depth), the presence of seismic scattering bodies with a low velocity signature was recognized (Kaneshima and Helffrich, 1999, 2003; Vinnik et al., 2001). As shown earlier, the most notable phase transition in major minerals in subducted slab and the surrounding mantle materials is the rutile to $CaCl_2$ transition of SiO_2 in subducted former oceanic crust under the P, T conditions of the middle part (~1600 km, corresponding to pressures of ~70 GPa; Tsuchiya et al., 2004c) of the lower mantle. A significant shear softening is expected to occur in St associated with this phase transition (Andrault et al., 1998; Karki et al., 1997b; Shieh et al., 2002). Thus, this transition in subducted basaltic material may explain the signatures of the scatterers observed in the middle part of the lower mantle. In contrast, the electronic spin transition in Mw in the upper to middle regions of the lower mantle may yield some variations in sound velocities, but these changes are rather gradual and probably seismologically invisible (e.g., Lin et al., 2013).

Tomographic imaging and other seismological studies demonstrate that only little anomalous changes in seismic velocities exist in the middle to lower part of the lower mantle except for regions related to subducted slabs and rising plumes (e.g., Grand et al., 1997; Mattern et al., 2005; Zhao, 2004). As shown in the previous section, no major phase changes have been reported in Mg-Pv, Ca-Pv, and Mw at pressures up to ~120 GPa, except for the slight distortion of cubic Ca-Pv to a tetragonal structure and the spin transitions in both Mg-Pv and Mw. It is expected that the transition in Ca-Pv may not occur at temperatures of the lower mantle, while the spin transitions should occur continuously over a wide pressure range as shown in **Figures 7** and **6**, respectively. Accordingly, both of these transitions would not cause any notable seismic velocity changes in this region, although further study is required to address the effects of the possible dissociation of Mw mentioned earlier. Thus, the relatively homogeneous nature in seismic velocity distributions in the middle to lower parts of the lower mantle is consistent with the absence of major phase transitions in the mantle material.

On the other hand, seismological, geochemical, and geodynamic studies suggest that there should be a chemically distinct regions at depths below 1500–2000 km, presumably due to iron-enrichment related to the primitive mantle materials or interaction with the rising hot plumes (e.g., Ishii and Tromp, 1999; Kellogg et al., 1999; Trampert et al., 2004). Attempts have been made to estimate the chemical composition of the lower mantle by mineral physics tests (e.g., Bina, 2003; Jackson and Rigden, 1998; Mattern et al., 2005), comparing calculated densities and bulk sound velocities of various compositions with those obtained seismologically. However, it is difficult to constrain the chemical composition of the lower mantle without reasonable estimations of thermal structures in this region and of shear properties of the relevant high-pressure phases. Actually, a wide range of chemical compositions from peridotite to chondrities can be accommodated for the acceptable geotherms, although anomalously high X_{Mg} (=Mg/(Mg+Fe)) and low X_{Pv} (=Si/(Mg+Fe)) and low X_{Mg} and high X_{Pv} are suggested in the uppermost and lowermost ~200 km of the lower mantle, respectively (Bina, 2003).

The possible iron and silica rich nature in the bottom part of the lower mantle may reflect the heterogeneous chemical composition and mineralogy of this region. These silicon-rich signatures can be explained by the presence of subducted oceanic crust materials in this region, which are denser than the surrounding pyrolitic or harzburgitic lower mantle materials, as shown in **Figure 11**, although the fraction of the basaltic component can significantly vary depending on its composition (Nakagawa et al., 2010). The $CaCl_2$–α-PbO_2 transition in SiO_2 is calculated to take place at 120–125 GPa and 2000–2500 K (Tsuchiya et al., 2004c), which should stabilize the SiO_2-bearing basaltic material in the D″ layer. Moreover, SiO_2 is also expected to exist in this region as a product of the reaction between the solid silicate Pv (or PPv) of the mantle and the molten Fe of the outer core (Knittle and Jeanloz, 1991).

In contrast, the Mg-rich and Si-poor refractory nature of the uppermost part of the lower mantle suggested by Bina (2003) could be due to the presence of accumulated harzburgite-rich bodies of the stagnant slabs (Fukao et al., 1992; Irifune et al.,

2008; Nakagawa et al., 2010; Ringwood and Irifune, 1988). This is mainly because harzburgite is less dense than pyrolite throughout the lower mantle, as is seen in **Figure 11**. Nevertheless, the density difference is not so large, and the thermal anomalies due to subduction of slabs or rising plumes may be more effective in circulation of the harzburgitic materials within the lower mantle.

2.03.5.3 PPv Transition and the D″ Layer

The bottom ~200 km of the lower mantle is known as a highly heterogeneous region on the basis of seismological observations, named as the D″ layer to distinguish it from the grossly homogeneous part of the lower mantle above (region D; Bullen, 1949). The horizontally and vertically heterogeneous nature of the D″ layer is primarily because this region is the chemical boundary layer between convective rocky mantle and molten iron core, which inevitably produces a large thermal boundary layer ($\Delta T > \sim 1000$ K; e.g., Williams, 1998) and accordingly yields active reactions of mantle and core materials (e.g., Knittle and Jeanloz, 1991), partial melting of mantle and slab materials (Lay et al., 2004), generation of hot mantle plumes (Garnero et al., 1998), etc. Various models have been proposed to account for the observed complex seismological signatures of D″ as reviewed by Garnero et al. (2004).

The recent finding of the Pv–PPv transition in $MgSiO_3$ has dramatically affected the conventional interpretations of the complex and heterogeneous features of the D″ layer. Many researchers in different research fields of Earth sciences, including mineral physics, seismology, geochemistry, mantle dynamics, etc., have started studies relevant to these topics, and a number of papers have been published immediately after the appearance of the first report on this issue (Murakami et al., 2004a). The rate of data accumulation is so fast and the relevant research fields so vast that we are unable to thoroughly evaluate all of these studies at this time. So, instead of discussing the origin of the D″ layer based on rather immature knowledge in these broad research fields, we herein summarize and examine currently available phase relations and some physical properties of the PPv in terms of high-pressure experimental and theoretical points of view. We will discuss the subject and speculate on the nature of the D″ layer within these mineral physics frameworks.

Now, what is most robust is that the Pv–PPv transition in $MgSiO_3$ does occur at pressures near the D″ layer on the basis of both high-pressure experiments and ab initio calculations. Also true is the fact that the latter phase adopts the crystal structure of $CaIrO_3$ type as evident from all of these studies. The density increase in Mg-Pv associated with this transition is most likely to be only 1.2–1.5% as constrained experimentally and predicted by ab initio calculations. The remarkable agreements among these independent studies on both experimental and theoretical bases strongly suggest that these should be regarded as facts beyond any doubts.

On the other hand, there are some uncertainties in the phase transition pressure and its temperature dependency. The pressures calculated with different scales in DAC experiments, even for those based on the EoS of gold, may differ by as much as 10–15 GPa at pressures of D″ layer (~120–136 GPa) due to the inaccuracy of the EoSs of pressure reference materials as discussed earlier (see **Figure 1**), and accordingly this transition could be realized only at pressures of the outer core (Shim et al., 2004). Moreover, uncertainties in temperature measurements in LHDAC at these very high pressure regions are fairly large, and are generally ±10–20% of the nominal values. These yield additional uncertainties of greater than 2–5 GPa in pressure measurements in LHDAC. Thus, the errors of the transition pressure can be ~±20 GPa for the Pv–PPv transition in $MgSiO_3$ within the current state-of-the-art LHDAC technology. Moreover, it is fair to say that the Clapeyron slope of this transition has been virtually unconstrained by LHDAC experiments.

In contrast, remarkably good agreement in phase transition pressures (~110 GPa, at 0 K) and the Clapeyron slopes (7–10 MPa K^{-1}) have been obtained in some independent ab initio calculations (Oganov and Ono, 2004; Tsuchiya et al., 2004a), and these are consistent with the experimental results and also with what are expected from seismological observations (Sidorin et al., 1999). The mutual agreement among the results of the ab initio calculations, however, does not warrant the validity of these values, as these authors used basically the same technique with only some relatively minor difference in computational methods and techniques. Thus, these results on the Pv–PPv phase boundary based on ab initio calculations should be further tested on the basis of experimental studies before they are regarded as robust ones.

Nevertheless, there is no strong evidence against the occurrence of the Pv–PPv transition at pressures about 120 GPa, with a Clapeyron slope of 7–10 MPa K^{-1}, and it is reasonable to tentatively take these values as realistic ones. It has been reported that such a large Clapeyron slope is expected to affect the thermal structure of the lower mantle and, thus, enhances the mantle convection and plume dynamics (Nakagawa and Tackley, 2004). For actual mantle compositions, effects of relatively minor elements such as Fe and Al should be taken into account, but as we mentioned earlier, these may have opposite effects in modifying the transition pressure which should cancel out each other. Actually, recent experimental results demonstrated that the Pv–PPv transition in peridotitic compositions occurs at pressures close to 120 GPa (Murakami et al., 2005; Ono et al., 2005d). Although a smeared-out transition is expected for this transition when some iron is incorporated in $MgSiO_3$ (Mao et al., 2004, 2005), these studies on the rock samples indicate that the pressure interval of the mixed phase region of Pv and PPv is not so large, suggesting the occurrence of a sharp boundary (Wysession et al., 1998). It is also demonstrated that the PPv phase in the peridotite composition is highly magnesium-rich relative to Mw (Murakami et al., 2005), whereas PPv is reported to favor iron compared with Pv in other experimental studies (Mao et al., 2004, 2005; cf. Kobayashi et al., 2005).

Another striking feature of PPv is its elasticity, as predicted by ab initio calculations (Iitaka et al., 2004; Oganov and Ono, 2004; Tsuchiya et al., 2004b). The predicted seismic wave speeds of PPv are slightly faster in V_P and V_S and slower in V_Φ than those of Pv at the transition P, T condition as typically observed at the D″ discontinuities (Lay et al., 2004). These velocity changes across the transition boundary seem to explain the enigmatic anticorrelated anomaly between V_S and V_Φ observed at the bottom of the mantle (Wentzcovitch et al.,

2006; Wookey et al., 2005). Also they can vary with changing the iron and aluminum contents in Pv and PPv (Tsuchiya and Tsuchiya, 2006).

Because of the peculiar crystal structure of PPv, which is highly compressible along the *b* direction, this phase is suggested to be elastically quite anisotropic. The ab initio studies also reported that PPv polycrystalline aggregates with lattice-preferred orientation (LPO) around some crystallographic directions produced by macroscopic stress appear to explain the observed anisotropic propagation of seismic waves in some regions of the D″ layer. In particular, some ab initio studies on high-temperature elasticity (Stackhouse et al., 2005a; Wentzcovitch et al., 2006) showed that the transversely isotropic aggregates of PPv can yield horizontally polarized S wave (SH) which travels faster than vertically poralized S wave (SV) at the lower mantle *P*, *T* condisitons, as observed underneath Alaska and central America (Lay et al., 2004). However, the peculiar nature of its shear elasticity suggests that the simple shear motion along the layered structure may not be applicable to the PPv phase at relevant pressures (Tsuchiya et al., 2004b). Moreover, it was predicted that Mw would have substantially large elastic anisotropy under the lower mantle conditions (Yamazaki and Karato, 2002), suggesting that the PPv phase may not be important in producing anisotropic nature in the D″ layer.

The most likely region, where the Pv–PPv transition play important roles in the D″ layer, is probably underneath some of the subduction zones, where the temperatures are expected to be relatively lower than that of the surrounding mantle. In these relatively cold regions in the D″ layer, it is known that a sharp discontinuity exists on the top of this layer, under which the highly anisotropic nature of propagation of SV and SH has also been recognized. If this discontinuity corresponds to the Pv–PPv transition, then one of the most likely features of this transition, that is, its large Clapeyron slope of $dP/dT = 7$–10 MPa K^{-1}, suggests that such discontinuity may not exist in warmer regions. For instance, if the temperature in the warmer region is higher than the cold areas by several hundred degrees (such a lateral temperature variation is very likely to exist in the CMB region), this transition would occur in the middle of the D″ layer. However, as the temperature is expected to increase sharply toward the CMB within the D″ layer, the geotherm in the warmer region may not cross the Pv–PPv phase boundary as illustrated in **Figure 12**, although some seismological observations would suggest not so high CMB temperatures in most regions of the lower mantle (Kawai and Tsuchiya, 2009). In contrast, it is interesting to see that there is a possibility that the geotherm in the colder region might cross the boundary twice, as suggested by recent computational modeling (Hernlund et al., 2005; Wookey et al., 2005).

Thus, if the transition pressure and the Clapeyron slope of the Pv–PPv transition predicted by ab initio calculations are correct, many of the observed features in the CMB region can be explained. In warmer regions such as underneath Hawaii or South Africa, this transition would not have any significant role in producing the peculiar features, such as the presence of an ultra-low velocity region or a large low velocity structure in these regions, which should be attributed to other phenomena, such as partial melting of the D″ layer material or chemical changes (e.g., Lay et al., 2004). Reactions between Mg-Pv in the warm regions with liquid iron may produce an iron-rich PPv phase in these regions, which could also contribute to the observed low velocities in these regions, as suggested by Mao et al. (2005). Such reactions between Pv (or PPv) and molten iron should be further explored experimentally to address the nature of the (ultra-) low velocity zones within the D″ layer.

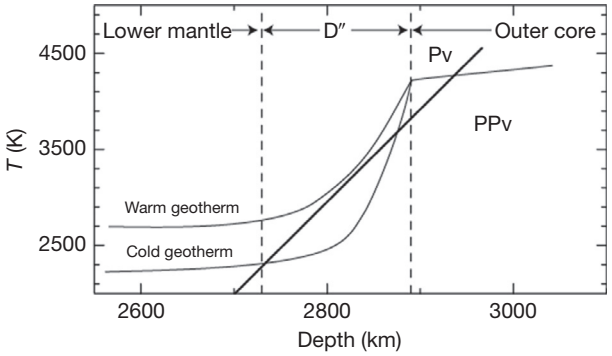

Figure 12 A schematic illustration of the plausible thermal structure at the bottom of the lower mantle, where a steep temperature gradient should be realized due to the formation of the thermal boundary layer. Only the sub-adiabatic cold geotherm may cross the Pv–PPv phase boundary, and the PPv phase may be sandwiched by Pv because of the shallow slope of this transition and the sharp temperature increase in this region. Reproduced from Hernlund JW, Thomas C, and Tackley PJ (2005) A doubling of the post-perovskite phase boundary and structure of the Earth's lowermost mantle. *Nature* 434: 882–886.

Over the past 30 years, the lowermost part of the Earth's mantle, the D″ layer, has been recognized as being a seismological anisotropic structure, whereas the rest of the lower mantle is nearly isotropic (Kendall and Silver, 1996; Mitchell and Helmberger, 1973; Panning and Romanowicz, 2004; Vinnik et al., 1998). Several observations suggest that the horizontally polarized shear wave (V_{SH}) is faster than the vertically polarized shear wave (V_{SV}) in most areas of the D″ layer (Kendall and Silver, 1996; Vinnik et al., 1998) except beneath the Africa and Pacific low-velocity provinces (Panning and Romanowicz, 2004). Several scenarios have been proposed for the splitting mechanism of the polarized shear waves in the D″ layer. One is the formation of shape-preferred orientations due to the alignment of fluid-inclusion or anisotropic atomic diffusion (Mainprice et al., 2000). Another, more efficient, origin can be found in the development of the LPO of (Mg,Fe)-PPv, which is thought to be the most abundant mineral in the D″ layer (Tsuchiya et al., 2004a) with a strong elastic anisotropy (Tsuchiya et al., 2004b), during plastic deformation with anisotropic shear response of the slip systems, such as dislocation creep or mechanical twinning. Although several high-pressure experiments have been performed to understand the plastic deformation mechanism of PPv (Hirose et al., 2010; Merkel et al., 2007; Miyagi et al., 2010, 2011; Okada et al., 2010), results are still largely controversial primarily due to experimental difficulty in determining the stable slip plane (Merkel et al., 2007; Miyagi et al., 2010). Most of these deformation experiments were conducted at room temperature, which is far lower than the geophysically relevant temperature of the D″ region of ~2500–3800 K (Brown and Shankland, 1981; Kawai and Tsuchiya, 2009). However, a high-temperature deformation experiment (Hirose et al., 2010) also shows the (001) plane as the stable slip plane of PPv. This slip mechanism can explain the

$V_{SH} > V_{SV}$ type polarization anisotropy observed in the D″ layer (Tsuchiya et al., 2004b).

Some theoretical studies also suggested contradicting results regarding the (100) or (110) slip planes (Oganov et al., 2005b) and (010) (Carrez et al., 2007) for PPv, primarily because these examined only particular structure modifications or calculated the GSF energies of limited slip planes. Another work of Fe-bearing Mg-PPv, on the other hand, calculated the GSF of several slip systems (Metsue and Tsuchiya, 2013) and found that pure and Fe-bearing $MgSiO_3$ PPv should demonstrate similar LPO patterns with a strong signature of the [100](001) slip system. Note again that an aggregate with this deformation texture is expected to produce a $V_{SH} > V_{SV}$ type polarization anisotropy, being consistent with seismological observations.

2.03.6 Summary

Recent advances in both experimental and computational techniques have enabled the quantitative study of phase transitions and mineral physics properties under the lower mantle *P*, *T* conditions. Although uncertainties in pressure and temperature are of the order of ~10% of the nominal values in typical experiments of LHDAC, this apparatus can now produce pressures and temperatures equivalent to those of the center of the Earth. In contrast, pressures available in KMA have long been limited to ~30 GPa in spite of its superiority in the accuracy of *P*, *T* measurements over LHDAC. However, recent developments in KMA using SD anvils expanded this pressure limit to the Mbar region, allowing detailed mineral physics studies down to the middle part of the lower mantle.

The accuracy of the mineral physics studies based on ab initio calculations has also been dramatically improved in the last decade. A variety of methods and techniques have been developed for the practical applications of DFT to mineral physics studies at very high pressure and temperature. As a result, remarkable agreements among the results from different research groups have been obtained for the phase transition pressures, elastic properties, etc., of some high-pressure phases under the lower mantle pressures. Thus, such mineral physics properties of high-pressure phases in the lower mantle can now be evaluated and cross-checked on the basis of the independent experimental studies using LHDAC and KMA and of ab initio calculations.

Phase transitions in major and minor minerals relevant to the mantle and subducted slabs have been studied by using the above independent methods, which clarified structural phase transitions in most of these minerals at pressures and temperatures characteristic of the lower mantle, although there remain some controversial results on the phase transition pressures, their temperature dependencies, element partitioning among the coexisting phases, etc. Although the elastic properties of high-pressure phases, particularly shear properties, have not been well documented under the lower mantle conditions, EoS parameters of some of these phases have successfully been determined by a combination of synchrotron source and KMA–LHDAC or by ab initio methods. Thus, the density changes in representative mantle and slab compositions can be accurately evaluated on the basis of the thermoelastic data on individual high-pressure phases and mineral proportion changes in these compositions.

The 660 km discontinuity has conventionally been interpreted in terms of the spinel–postspinel phase transition in Mg_2SiO_4. However, results of the recent experimental, seismological, and geodynamics studies do not seem to be totally consistent with this interpretation. The presence of either a basaltic or a harzburgite layer, as a result of accumulation of subducted slab materials, may explain such inconsistency and the complex structure near the 660 km discontinuity. The validity of this and other classes of mineralogical models relevant to the origin of the 660 km discontinuity can be evaluated on the basis of mineral physics tests, when accurate elastic wave velocity data are accumulated for the pyrolite, harzburgite, MORB, and other subducted materials under the *P*, *T* conditions corresponding to these depths.

The middle part of the lower mantle is believed to be generally homogeneous in both mineralogy and chemistry, as compared with those in the uppermost and lowermost parts of the lower mantle. No major phase transitions are expected to occur in the subducted slab lithologies and the surrounding mantle under the *P*, *T* conditions of this part of the lower mantle, except for the rutile to $CaCl_2$ transition in SiO_2 and electronic spin transitions in Mw and Pv. The seismic scatterers of presumably flat bodies found in the middle part of the lower mantle should be related to this phase transition in the former subducted oceanic crust, which may subduct into the deep lower mantle once it passes the density crossover near the 660 km discontinuity. Thus, some parts of the basaltic component of the slab may ultimately reach the bottom of the lower mantle because of its higher density relative to the mantle materials throughout the lower mantle. In contrast, a harzburgite-rich layer may be present around the 660 km discontinuity as a result of accumulation of main bodies of stagnant slabs in this region. However, as the density difference between this layer and the surrounding mantle is not large, thermal effects should be predominant over the chemical effects in gravitational stability of such a layer, leading to possible generation of plumes in the region.

The Pv–PPv transition should have significant implications for the structure, properties, and dynamics of the D″ layer. Some properties, such as Clapeyron slope, transition pressure, elastically anisotropic nature, and density increase relevant to the Pv–PPv transition seem to be consistent with the seismologically observed signatures in some regions of the D″ layer. Further detailed and more accurate experimental studies on this transition are required based on independent techniques using KMA or LHDAC with improved accuracy, in addition to the theoretical studies, to understand the nature of this region of the lower mantle.

Acknowledgments

We thank J. Tsuchiya for her help and fruitful discussion in preparation of the manuscript. Comments by D. Zhao, T. Inoue, A. Yamada, T. Tange, Y. Wang, and an anonymous reviewer are also sincerely acknowledged.

References

Akahama Y, Kawamura H, and Singh AK (2002) The equation of state of Bi and cross-checking of Au and Pt scales to megabar pressure. *Journal of Physics: Condensed Matter* 14: 11495–11500.

Akahama Y, Kawamura H, and Singh AK (2004) A comparison of volume compressions of silver and gold to 150 GPa. *Journal of Applied Physics* 95: 4767–4771.

Akaogi M, Hamada Y, Suzuki T, Kobayashi M, and Okada M (1999) High pressure transitions in the system $MgAl_2O_4$–$CaAl_2O_4$: A new hexagonal aluminous phase with implication for the lower mantle. *Physics of the Earth and Planetary Interiors* 115: 67–77.

Akaogi M, Haraguchi M, Yaguchi M, and Kojitani H (2009) High-pressure phase relations and thermodynamic properties of $CaAl_4Si_2O_{11}$ CAS phase. *Physics of the Earth and Planetary Interiors* 173: 1–6.

Akaogi M and Ito E (1993) Refinement of enthalpy measurement of $MgSiO_3$ perovskite and negative pressure–temperature slopes for perovskite-forming reactions. *Geophysical Research Letters* 20: 1839–1842.

Akber-Knutson S, Steinle-Neumann G, and Asimow PD (2005) Effect of Al on the sharpness of the $MgSiO_3$ perovskite to post-perovskite phase transition. *Geophysical Research Letters* 32. http://dx.doi.org/10.1029/2005GL023192, L14303.

Alfé D, Alfredsson M, Brodholt J, Gillan MJ, Towler MD, and Needs RJ (2005) Quantum Monte Carlo calculations of the structural properties and the B1–B2 phase transition of MgO. *Physical Review B* 72: 014114.

Anderson DL (1979) The upper mantle: Eclogite? *Geophysical Research Letters* 6: 433–436.

Anderson DL (1989) Composition of the Earth. *Science* 243: 367–370.

Anderson DL and Bass JD (1986) Transition region of the Earth's upper mantle. *Nature* 320: 321–328.

Anderson OL, Isaak DG, and Yamamoto S (1989) Anharmonicity and the equation of state for gold. *Journal of Applied Physics* 65: 1534–1543.

Andrault D, Angel RJ, Mosenfelder JL, and Le Bihan T (2003) Equation of state of stishovite to lower mantle pressures. *American Mineralogist* 88: 1261–1265.

Andrault D, Fiquet G, Guyot F, and Hanfland M (1998) Pressure-induced Landau-type transition in stishovite. *Science* 282: 720–724.

Andrault D, Munoz M, Bolfan-Casanova N, et al. (2010) Experimental evidence for perovskite and post-perovskite coexistence throughout the whole D″ region. *Earth and Planetary Science Letters* 293: 90–96.

Anisimov VI, Zaanen J, and Andersen OK (1991) Band theory and Mott insulators: Hubbard U instead of Stoner I. *Physical Review B* 44: 943–954.

Antonangeli D, Siebert J, Aracne CM, et al. (2011) Spin crossover in ferropericlase at high pressure: A seismologically transparent transition? *Science* 331: 64–67.

Badro J, Fiquet G, Guyot F, et al. (2003) Iron partitioning in Earth's mantle: Toward a deep lower mantle discontinuity. *Science* 300: 789–791.

Badro J, Rueff J-P, Vankó G, Monaco G, Fiquet G, and Guyot F (2004) Electronic transitions in perovskite: Possible nonconvecting layers in the lower mantle. *Science* 305: 383–386.

Badro J, Struzhkin VV, Shu J, et al. (1999) Magnetism in FeO at megabar pressures from X-ray emission spectroscopy. *Physical Review Letters* 83: 4101–4104.

Bagno P, Jepsen O, and Gunnarsson O (1989) Ground-state properties of third-row elements with nonlocal density functionals. *Physical Review B* 40: 1997–2000.

Baroni S, de Gironcoli S, Corso AD, and Giannozzi P (2001) Phonons and related crystal properties from density-functuional perturbation theory. *Reviews of Modern Physics* 73: 515–562.

Baroni S, Giannozzi P, and Testa A (1987) Green's-function approach to linear response in solids. *Physical Review Letters* 58: 1861–1864.

Beck P, Gillet P, Gautron L, Daniel I, and El Goresy A (2004) A new natural high-pressure (Na, Ca)-hexaluminosilicate $[(Ca_xNa_{1-x})Al_{3+x}Si_{3-x}O_{11}]$ in shocked Martian meteorites. *Earth and Planetary Science Letters* 219: 1–12.

Biellmann C, Gillet P, Guyot F, Peyronneau J, and Reyard B (1993) Experimental evidence for carbonate stability in Earth's lower mantle. *Earth and Planetary Science Letters* 118: 31–41.

Bina CR (2003) Seismological constraints upon mantle composition. In: Carlson R (ed.) *Treatise on Geochemistry*, vol. 2, pp. 39–59. Amsterdam: Elsevier Science Publishing.

Birch F (1952) Elasticity and constitution of the Earth's interior. *Journal of Geophysical Research* 57: 227–286.

Bolfan-Casanova N, Andrault D, Armiguet E, and Guignot N (2009) Equation of state and post-stishovite transformation of Al-bearing silica up to 100 GPa and 3000 K. *Physics of the Earth and Planetary Interiors* 174: 70–77.

Brown JM and Shankland TJ (1981) Thermodynamic parameters in the Earth as determined from seismic profiles. *Geophysical Journal of the Royal Astronomical Society* 66: 579–596.

Bullen KE (1949) Compressibility-pressure hypothesis and the Earth's interior. *Geophysical Supplement of Monthly Notices of the Royal Astronomical Society* 5: 355–368.

Camarano F, Romanowicz B, Stixrude L, Lithgow-Bertelloni C, and Xu W (2009) Inferring the thermochemical structure of the upper mantle from seismic data. *Geophysical Journal International* 179: 1169–1185.

Caracas R and Boffa Ballaran T (2010) Elasticity of (K, Na)$AlSi_3O_8$ hollandite from lattice dynamics calculations. *Physics of the Earth and Planetary Interiors* 181: 21–26.

Caracas R and Cohen RE (2005a) Prediction of a new phase transition in Al_2O_3 at high pressures. *Geophysical Research Letters* 32: L06303. http://dx.doi.org/10.1029/2004GL022204.

Caracas R and Cohen RE (2005b) Effect of chemistry on the stability and elasticity of the perovskite and post-perovskite phases in the $MgSiO_3$–$FeSiO_3$–Al_2O_3 system and implications for the lowermost mantle. *Geophysical Research Letters* 32: L16310. http://dx.doi.org/10.1029/2005GL023164.

Caracas R, Wentzcovitch R, Price GD, and Brodholt J (2005) $CaSiO_3$ perovskite at lower mantle pressures. *Geophysical Research Letters* 32: L06306. http://dx.doi.org/10.1029/2004GL022144.

Carrez P, Ferré D, and Cordier P (2007) Implications for plastic flow in the deep mantle from modelling dislocations in $MgSiO_3$ minerals. *Nature* 446: 68–70.

Catalli K, Shim S-H, and Prakapenka V (2009) Thickness and Clapeyron slope of the post-perovskite boundary. *Nature* 462: 782–786.

Catti M (2001) High-pressure stability, structure and compressibility of *Cmcm*-$MgAl_2O_4$: An *ab initio* study. *Physics and Chemistry of Minerals* 28: 729–736.

Chizmeshya AVG, Wolf GH, and McMillan PF (1996) First principles calculation of the equation-of-state, stability, and polar optic modes of $CaSiO_3$ perovskite. *Geophysical Research Letters* 23: 2725–2728.

Chudinovskikh L and Boehler R (2001) High-pressure polymorphs of olivine and the 660-km seismic discontinuity. *Nature* 411: 574–577.

Cococcioni M and de Gironcoli S (2005) Linear response approach to the calculation of the effective interaction parameters in the LDA + U method. *Physical Review B* 71: 035105.

Cohen RE, Mazin II, and Isaak DG (1997) Magnetic collapse in transition metal oxides at high pressure: Implications for the Earth. *Science* 275: 654–657.

Crowhurst JC, Brown JM, Goncharov AF, and Jacobsen SD (2008) Elasticity of (Mg,Fe)O through the spin transition of iron in the lower mantle. *Science* 319: 451–453.

Davis GF (1998) Plates, plumes, mantle convection, and mantle evolution. In: Jackson I (ed.) *The Earth's Mantle*, pp. 228–258. New York: Cambridge University Press.

Dekura H, Tsuchiya T, and Tsuchiya J (2013) Ab initio lattice thermal conductivity of $MgSiO_3$ perovskite as found in the Earth's lower mantle. *Physical Review Letters* 110: 025904.

Demuth Th, Jeanvoine Y, Hafner J, and Ángyán JG (1999) Polymorphism in silica studied in the local density and generalized-gradient approximations. *Journal of Physics: Condensed Matter* 11: 3833–3874.

Deng L, Liu X, Liu H, and Dong J (2010) High-pressure phase relations in the composition of albite $NaAlSi_3O_8$ conatrained by an *ab initio* and quasi-harmonic Debye model, and their implications. *Earth and Planetary Science Letters* 298: 427–433.

Dubrovinsky LS, Dubrovinskaia NA, Saxena SK, et al. (2000) Stability of ferropericlase in the lower mantle. *Science* 289: 430–432.

Dubrovinsky LS, Dubrovinskaia NA, Saxena SK, et al. (2001) Pressure-induced transformations of cristobalite. *Chemical Physics Letters* 333: 264–270.

Dubrovinsky LS, Saxena SK, Lazor P, et al. (1997) Experimental and theoretical identification of a new high-pressure phase of silica. *Nature* 388: 362–365.

Duffy TS and Anderson DL (1989) Seismic velocities in mantle minerals and the mineralogy of the upper mantle. *Journal of Geophysical Research* 94: 1895–1912.

Duffy TS, Hemley RJ, and Mao H-K (1995) Equation of state and shear strength at multimegabar pressures: Magnesium oxide to 227 GPa. *Physical Review Letters* 74: 1371–1374.

Dziewonski AM and Anderson DL (1981) Preliminary reference Earth model. *Physics of the Earth and Planetary Interiors* 25: 297–356.

Fei Y and Mao H-K (1994) *In situ* determination of the NiAs phase of FeO at high pressure and high temperature. *Science* 266: 1678–1680.

Fei Y, Van Orman J, Li J, et al. (2004) Experimentally determined postspinel transformation boundary in Mg_2SiO_4 using MgO as an internal pressure standard and its geophysical implications. *Journal of Geophysical Research* 109: B02305.

Ferroir T, Yagi T, Onozawa T, et al. (2006) Equation of state and phase transition in $KAlSi_3O_8$ hollandite at high pressure. *American Mineralogist* 91: 327–332.

Fiquet G, Dewaele A, Andrault D, Kunz M, and Bihan TL (2000) Thermoelastic properties and crystal structure of $MgSiO_3$ perovskite at lower mantle pressure and temperature conditions. *Geophysical Research Letters* 27: 21–24.

Fiquet A, Guyot F, Kunz M, Matas J, Andrault D, and Hanfland M (2002) Structural refinements of magnesite at very high pressure. *American Mineralogist* 87: 1261–1265.

Fiquet G, Richet P, and Montagnac G (1999) High-temperature thermal expansion of lime, periclase, corundum and spinel. *Physics and Chemistry of Minerals* 27: 103–111.

Fischer RA, Campbell AJ, Lord OT, Shofner GA, Dera P, and Prakapenka VB (2011) Phase transition and metallization of FeO at high pressures and temperatures. *Geophysical Research Letters* 38. http://dx.doi.org/10.1029/2011GL049800.

Flanagan MP and Shearer PM (1998) Global mapping of topography on transition zone velocity discontinuities by stacking SS precursors. *Journal of Geophysical Research* 103: 2673–2692.

Frost DJ and Fei Y (1998) Stability of phase D at high pressure and high temperature. *Journal of Geophysical Research* 103: 7463–7474.

Frost DJ and Langenhorst F (2002) The effect of Al_2O_3 on Fe–Mg partitioning between magnesiowustite and magnesium silicate perovskite. *Earth and Planetary Science Letters* 199: 227–241.

Fukao Y, Obayashi M, Inoue H, and Nenbai M (1992) Subducting slabs stagnant in the mantle transition zone. *Journal of Geophysical Research* 97: 4809–4822.

Fukao Y, Widiyantoro S, and Obayashi M (2001) Stagnant slabs in the upper and lower mantle transition region. *Reviews of Geophysics* 39: 291–323.

Fukui H, Tsuchiya T, and Baron AQR (2012) Lattice dynamics calculations for ferropericlase with internally consistent LDA + *U* method. *Journal of Geophysical Research* 117. http://dx.doi.org/10.1029/2012JB009591.

Funamori N and Jeanloz R (1997) High-pressure transformation of Al_2O_3. *Science* 278: 1109–1111.

Funamori N, Jeanloz R, Nguyen JH, et al. (1998) High-pressure transformations in $MgAl_2O_4$. *Journal of Geophysical Research* 103: 20813–20818.

Funamori N, Yagi T, Utsumi W, Kondo T, and Uchida T (1996) Thermoelastic properties of $MgSiO_3$ perovskite determined by *in situ* X-ray observations up to 30 GPa and 2000 K. *Journal of Geophysical Research* 101: 8257–8269.

Gaffney ES and Anderson DL (1973) Effect of low-spin Fe^{2+} on the composition of the lower mantle. *Journal of Geophysical Research* 78: 7005–7014.

Garnero EJ, Maupin V, Lay T, and Fouch MJ (2004) Variable azimuthal anisotropy in Earth's lowermost mantle. *Science* 306: 259–261.

Garnero EJ, Revenaugh JS, Williams Q, Lay T, and Kellogg LH (1998) Ultralow velocity zone at the core-mantle boundary. In: Gurnis M, Wysession M, Knittle E, and Buffett B (eds.) *The Core-Mantle Boundary Region*, pp. 319–334. Washington, DC: American Geophysical Union.

Gautron L, Angel RJ, and Miletich R (1999) Structural characterization of the high-pressure phase $CaAl_4Si_2O_{11}$. *Physics and Chemistry of Minerals* 27: 47–51.

Gautron L, Daniel I, Beck P, Gulgnot N, Andrault D, and Greaux S (2005) On the track of 5-fold silicon signature in the high pressure CAS phase $CaAl_4Si_2O_{11}$. *EOS Transaction AGU* 86, Fall Meeting Supplement 52, Abstract MR23C-0087.

Gillet P (1993) Stability of magnesite ($MgCO_3$) at mantle pressure and temperature conditions: A Raman spectroscopic study. *American Mineralogist* 78: 1328–1331.

Gillet P, Chen M, Dubrovinsky LS, and El Goresy A (2000) Natural $NaAlSi_3O_8$-hollandite in the shocked Sixiangkou meteorite. *Science* 287: 1633–1636.

Grand S, van der Hilst R, and Widiyantoro S (1997) Global seismic tomography: A snap shot of convection in the Earth. *GSA Today* 7: 1–7.

Greaux S, Nishiyama N, Kono Y, et al. (2011) Phase transformations of $Ca_3Al_2Si_3O_{12}$ grossular garnet to the depths of the Earth's mantle transition zone. *Physics of the Earth and Planetary Interiors* 185: 89–99.

Green DH, Hibberson WO, and Jaques AL (1979) Petrogenesis of mid-ocean ridge basalts. In: McElhinny MW (ed.) *The Earth: Its Origin, Structure and Evolution*, pp. 269–299. London: Academic Press.

Hamann DR (1996) Generalized gradient theory for silica phase transitions. *Physical Review Letters* 76: 660–663.

Hamann DR (1997) H_2O hydrogen bonding in density-functional theory. *Physical Review B* 55: R10157–R10160.

Hamaya N, Okabe N, Yamanaka M, Yagi T, and Shimomura O (1996) Performance of different types of detectors in a high-pressure x-ray study of phase transition. *High Pressure Research* 14: 287–294.

Hart SR and Zindler A (1986) In search for a bulk Earth composition. *Chemical Geology* 57: 247–267.

Heinz DL and Jeanloz R (1984) The equation of state of the gold calibration standard. *Journal of Applied Physics* 55: 885–893.

Helffrich G and Wood B (2001) The Earth's mantle. *Nature* 412: 501–507.

Hernlund JW, Thomas C, and Tackley PJ (2005) A doubling of the post-perovskite phase boundary and structure of the Earth's lowermost mantle. *Nature* 434: 882–886.

Higo Y, Inoue T, Irifune T, Funakoshi K-I, and Li B (2008) Elastic wave velocities of $(Mg_{0.91}Fe_{0.09})_2SiO_4$ ringwoodite under P–T conditions of the mantle transition region. *Physics of the Earth and Planetary Interiors* 3–4: 167–174.

Hirao N, Ohtani E, Kondo T, Sakai T, and Kikegawa T (2008) Hollandite II phase in $KAlSi_3O_8$ as a potential host mineral of potassium in the Earth's lower mantle. *Physics of the Earth and Planetary Interiors* 166: 97–104.

Hirose K (2002) Phase transition in pyrolitic mantle around 670-km depth: Implications for upwelling of plumes from the lower mantle. *Journal of Geophysical Research* 107: 2078. http://dx.doi.org/10.1029/2001JB000597.

Hirose K, Fei Y, Ma Y, and Mao H-K (1999) The fate of subducted basaltic crust in the Earth's lower mantle. *Nature* 397: 53–56.

Hirose K, Nagaya Y, Merkel S, and Ohishi Y (2010) Deformation of $MnGeO_3$ post-perovskite at lower mantle pressure and temperature. *Geophysical Research Letters* 37. http://dx.doi.org/10.1029/2010GL044977.

Hirose K, Takafuji N, Fujino K, Sehieh SR, and Duffy TS (2008) Iron partitioning between perovskite and post-perovskite: A transmission electron microscope study. *American Mineralogist* 93: 1678–1681.

Hirose K, Takafuji N, Sata N, and Ohishi Y (2005) Phase transition and density of subducted MORB crust in the lower mantle. *Earth and Planetary Science Letters* 237: 239–251.

Hohenberg P and Kohn W (1964) Inhomogeneous electron gas. *Physics Review* 136: B364–B871.

Holmes NC, Moriarty JA, Gathers GR, and Nellis WJ (1989) The equation of state of platinum to 660 GPa (6.6 Mbar). *Journal of Applied Physics* 66: 2962–2967.

Hsu H, Blaha P, Cococcioni M, and Wentzcovitch RM (2011) Spin-state crossover and hyperfine interactions of ferric iron in $MgSiO_3$ perovskite. *Physical Review Letters* 106: 118501.

Ice GE, Budai JD, and Pang WL (2010) The race to x-ray microbeam and nanobeam science. *Science* 334: 1234–1239.

Ichikawa H, Kawai K, Yamamoto S, and Kamayama M (2013) Supply rate of continental materials to the deep mantle through subduction channels. *Tectonophysics* 592: 46–52.

Iitaka T, Hirose K, Kawamura K, and Murakami M (2004) The elasticity of the $MgSiO_3$ post-perovskite phase in the Earth's lowermost mantle. *Nature* 430: 442–444.

Imada S, Hirose K, and Ohishi Y (2011) Stabilities of NAL and Ca-ferrite-type phases on the join $NaAlSiO_4$–$MgAl_2O_4$ at high pressure. *Physics and Chemistry of Minerals* 38: 557–560.

Irifune T (1993) Phase transformations in the earth's mantle and subducting slabs: Implications for their compositions, seismic velocity and density structures and dynamics. *Island Arc* 2: 55–71.

Irifune T (1994) Absence of an aluminous phase in the upper part of the Earth's lower mantle. *Nature* 370: 131–133.

Irifune T (2002) Application of synchrotron radiation and Kawai-type apparatus to various studies in high-pressure mineral physics. *Mineralogical Magazine* 66: 769–790.

Irifune T, Fujino K, and Ohtani E (1991) A new high-pressure form of $MgAl_2O_4$. *Nature* 349: 409–411.

Irifune T, Higo Y, Inoue T, Kono Y, Ohfuji H, and Funakoshi K-I (2008) Sound velocities of majorite garnet and the composition of the mantle transition region. *Nature* 451: 814–817.

Irifune T, Isobe F, and Shinmei T (2013) A novel large-volume Kawai-type apparatus and its application to the synthesis of sintered bodies of nano-polycrystalline diamond. *Physics of the Earth and Planetary Interiors*. http://dx.doi.org/10.1016/j.pepi.2013.09.007.

Irifune T, Isshiki M, and Sakamoto S (2005) Transmission electron microscope observation of the high-pressure form of magnesite retrieved from laser heated diamond anvil cell. *Earth and Planetary Science Letters* 239: 98–105.

Irifune T, Koizumi T, and Ando J (1996a) An experimental study of the garnet-perovskite transformation in the system $MgSiO_3$–$Mg_3Al_2Si_3O_{12}$. *Physics of the Earth and Planetary Interiors* 96: 147–157.

Irifune T, Kuroda K, Funamori N, et al. (1996b) Amorphization of serpentine at high pressure and high temperature. *Science* 272: 1468–1470.

Irifune T, Kubo N, Isshiki M, and Yamasaki Y (1998a) Phase transformations in serpentine and transportation of water into the lower mantle. *Geophysical Research Letters* 25: 203–206.

Irifune T, Nishiyama N, Kuroda K, et al. (1998b) The postspinel phase boundary in Mg_2SiO_4 determined by *in situ* X-ray diffraction. *Science* 279: 1698–1700.

Irifune T, Kurio A, Sakamoto S, Inoue T, and Sumiya H (2003) Ultrahard polycrystalline diamond from graphite. *Nature* 421: 599–600.

Irifune T and Ringwood AE (1987) Phase transformations in a harzburgite composition to 26 GPa: Implications for dynamical behaviour of the subducting slab. *Earth and Planetary Science Letters* 86: 365–376.

Irifune T and Ringwood AE (1993) Phase transformations in subducted oceanic crust and buoyancy relationships at depths of 600–800 km in the mantle. *Earth and Planetary Science Letters* 117: 101–110.

Irifune T, Ringwood AE, and Hibberson WO (1994) Subduction of continental crust and terrigenous and pelagic sediments: An experimental study. *Earth and Planetary Science Letters* 126: 351–368.

Irifune T, Shinmei T, McCammon CA, Miyajima N, Rubie DC, and Frost DJ (2010) Iron partitioning and density changes of pyrolite in Earth's lower mantle. *Science* 327: 193–195.

Ishii T, Kojitani H, and Akaogi M (2012) High-pressure phase transitions and subduction behavior of continental crust at pressure–temperature conditions up to the upper part of the lower mantle. *Earth and Planetary Science Letters* 357–358: 31–41.

Ishii M and Tromp J (1999) Normal-mode and free-air gravity constraints on lateral variations in velocity and density of Earth's mantle. *Science* 285: 1231–1236.

Isshiki M, Irifune T, Hirose K, et al. (2004) Stability of magnesite and its high-pressure form in the lowermost mantle. *Nature* 427: 60–63.

Ito E (2012) Development of the Kawai-type multi-anvil apparatus (KMA) and its application to high pressure earth science. *Journal of Physics: Conference Series* 377, Art. No. 012001.

Ito E, Katsura T, Aizawa Y, Kawabe K, Yokoshi S, and Kubo A (2005) High-pressure generation in the Kawai-type apparatus equipped with sintered diamond anvils: Application to the wurtzite–rocksalt transformation in GaN. In: Chen J, Wang Y, Duffy TS, Shen G, and Dobrzhinetskaya LF (eds.) *Advances in High-Pressure Technology for Geophysical Applications*, pp. 451–460. Amsterdam: Elsevier Science.

Ito E, Kubo A, Katsura T, Akaogi M, and Fujita T (1998) High-pressure phase transition of pyrope ($Mg_3Al_2Si_3O_{12}$) in a sintered diamond cubic anvil assembly. *Geophysical Research Letters* 25: 821–824.

Ito E and Takahashi E (1989) Post-spinel transformations in the system. Mg_2SiO_4–Fe_2SiO_4 and some geophysical implications. *Journal of Geophysical Research* 94: 10637–10646.

Jackson I, Khanna SK, Revcolevschi A, and Berthon J (1990) Elasticity, shear-mode softening and high-pressure polymorphism of Wüstite ($Fe_{1-x}O$). *Journal of Geophysical Research* 95: 21671–21685.

Jackson I and Rigden SM (1998) Composition and temperature of the Earth's mantle: Seismological models interpreted through experimental studies of the Earth materials. In: Jackson I (ed.) *The Earth's Mantle*, pp. 405–460. New York: Cambridge University Press.

Jackson JM, Sturhahn W, Shen G, et al. (2005) A synchrotron Mössbauer spectroscopy study of (Mg,Fe)SiO_3 perovskite up to 120 GPa. *American Mineralogist* 90: 199–205.

Jacobsen SD, Reichmann HJ, Spetzler HA, et al. (2002) Structure and elasticity of single crystal (Fe, Mg)O and a new method of generating shear waves for gigahertz ultrasonic interferometry. *Journal of Geophysical Research* 107: 1–14, 10.1029/2001JB000490.

Jamieson JC, Fritz JN, and Manghnani MH (1982) Pressure measurement at high temperature in x-ray diffraction studies: Gold as a primary standard. In: Akimoto S and Manghnani MH (eds.) *High-Pressure Research in Geophysics*, pp. 27–48. Tokyo: Center for Academic Publications.

Jeanloz R and Thompson AB (1983) Phase transitions and mantle discontinuities. *Reviews of Geophysics and Space Physics* 21: 51–74.

Kaneshima S (2003) Small scale heterogeneity at the top of the lower mantle around the Mariana slab. *Earth and Planetary Science Letters* 209: 85–101.

Kaneshima S and Helffrich G (1999) Dipping low-velocity layer in the mid-lower mantle: Evidence for geochemical heterogeneity. *Science* 283: 1888–1891.

Kaneshima S and Helffrich G (2003) Subparallel dipping heterogeneities in the mid-lower mantle. *Journal of Geophysical Research* 108: 2272. http://dx.doi.org/10.1029/2001JB001596.

Karato S (1997) On the separation of crustal component from subducted oceanic lithosphere near the 660 km discontinuity. *Physics of the Earth and Planetary Interiors* 99: 103–111.

Karki BB and Crain J (1998) First-principles determination of elastic properties of $CaSiO_3$ perovskite at lower mantle pressures. *Geophysical Research Letters* 25: 2741–2744.

Karki BB, Stixrude L, and Crain J (1997a) *Ab initio* elasticity of three high-pressure polymorphs of silica. *Geophysical Research Letters* 24: 3269–3272.

Karki BB, Warren MC, Stixrude L, Clark SJ, Ackland GJ, and Crain J (1997b) *Ab initio* studies of high-pressure structural transformations in silica. *Physical Review B* 55: 3465–3471.

Karki BB, Wentzcovitch RM, de Gironcoli S, and Baroni S (1999) First-principles determination of elastic anisotropy and wave velocities of MgO at lower mantle conditions. *Science* 286: 1705–1707.

Karki BB, Wentzcovitch RM, de Gironcoli S, and Baroni S (2000a) High-pressure lattice dynamics and themoelasticity of MgO. *Physical Review B* 61: 8793–8800.

Karki BB, Wentzcovitch RM, de Gironcoli S, and Baroni S (2000b) *Ab initio* lattice dynamics of $MgSiO_3$ perovskite at high pressure. *Physical Review B* 62: 14750–14756.

Katsura T and Ito E (1996) Determination of Fe–Mg partitioning between perovskite and magnesiowüstite. *Geophysical Research Letters* 23: 2005–2008.

Katsura T, Yamada H, Shinmei T, et al. (2003) Post-spinel transition in Mg_2SiO_4 determined by high P–T *in situ* X-ray diffractometry. *Physics of the Earth and Planetary Interiors* 136: 11–24.

Kawai N and Endo S (1970) The generation of ultrahigh hydrostatic pressures by a split sphere apparatus. *Review of Scientific Instruments* 41: 1178–1181.

Kawai K and Tsuchiya T (2009) Temperature profile in the lowermost mantle from seismological and mineral physics joint modeling. *Proceedings of the National Academy of Sciences of the United States of America* 106: 22119–22123.

Kawai K and Tsuchiya T (2012) Phase stability and elastic properties of the NAL and CF phases in the $NaMg_2Al_5SiO_{12}$ system from first principles. *American Mineralogist* 97: 305–314.

Kawai K and Tsuchiya T (2013) First-principles study on the high-pressure phase transition and elasticity of $KAlSi_3O_8$ hollandite. *American Mineralogist* 98: 207–218.

Kawai K, Yamamoto S, Tsuchiya T, and Maruyama S (2013) The second continent: Existence of granitic continental materials around the bottom of the mantle transition zone. *Geoscience Frontiers* 4: 1–6.

Kawakatsu H and Niu F (1994) Seismic evidence for a 920 km discontinuity in the mantle. *Nature* 371: 301–305.

Kellogg LH, Hager BH, and van der Hilst RD (1999) Compositional stratification in the deep mantle. *Science* 283: 1881–1884.

Kendall J-M and Silver PG (1996) Constraints from seismic anisotropy on the nature of the lowermost mantle. *Nature* 381: 409–412.

Kesson SE, Fitz Gerald JD, and Shelley JM (1998) Mineralogy and dynamics of a pyrolite lower mantle. *Nature* 393: 252–255.

Kiefer B, Stixrude L, and Wentzcovitch RM (2002) Elasticity of (Mg,Fe)SiO_3-perovskite at high pressure. *Geophysical Research Letters* 29: 1539. http://dx.doi.org/10.1029/2002GL014683.

Kingma KJ, Cohen RE, Hemley RJ, and Mao HK (1995) Transformation of stishovite to a denser phase at lower-mantle pressures. *Nature* 374: 243–246.

Knittle E and Jeanloz R (1991) Earth's core-mantle boundary: Results of experiments at high pressure and temperatures. *Science* 251: 1438–1443.

Kobayashi Y, Kondo T, Ohtani E, et al. (2005) Fe–Mg partitioning between (Mg,Fe)SiO_3 post-perovskite, perovskite, and magnesiowüstite in the Earth's lower mantle. *Geophysical Research Letters* 32: L19301. http://dx.doi.org/10.1029/2005GL023257.

Kohn W and Sham LJ (1965) Self-consistent equation including exchange and correlation effects. *Physics Review* 140: A1133–A1138.

Kondo T, Ohtani E, Hirao N, Yagi T, and Kikegawa T (2004) Phase transitions of (Mg,Fe)O at megabar pressures. *Physics of the Earth and Planetary Interiors* 143–144: 201–213.

Kono Y, Irifune T, Higo Y, et al. (2010) P–V–T relation of MgO derived by simultaneous elastic wave velocity and *in situ* measurements: A new pressure scale for the mantle transition region. *Physics of the Earth and Planetary Interiors* 183: 196–211.

Kono Y, Irifune T, Ohfuji H, Higo Y, and Funakoshi K-I (2012) Sound velocities of MORB and absence of a basaltic layer in the mantle transition region. *Geophysical Research Letters* 39. http://dx.doi.org/10.1029/2012GL054009.

Kruger F, Banumann M, Scherbaum F, and Weber M (2001) Mid mantle scatterers near the Mariana slab detected with a double array method. *Geophysical Research Letters* 28: 667–670.

Kubo T, Ohtani E, Kondo T, et al. (2002) Metastable garnet in oceanic crust at the top of the lower mantle. *Nature* 420: 803–806.

Kudoh Y, Nagase T, Mizohata H, and Ohtani E (1997) Structure and crystal chemistry of phase G, a new hydrous magnesium silicate synthesized at 22 GPa and 1050 °C. *Geophysical Research Letters* 24: 1051–1054.

Kurashina T, Hirose K, Ono S, Sata N, and Ohishi Y (2004) Phase transition in Al-bearing $CaSiO_3$ perovskite: Implications for seismic discontinuities in the lower mantle. *Physics of the Earth and Planetary Interiors* 145: 67–74.

Kuroda K and Irifune T (1998) Observation of phase transformations in serpentine at high pressure and high temperature by *in situ* X ray diffraction measurements. In: Manghnani MH and Yagi T (eds.) *High Pressure-Temperature Research: Properties of Earth and Planetary Materials*, pp. 545–554. Washington, DC: American Geophysical Union.

Lakshtanov D, Sinogeikin SV, Litasov KD, et al. (2007) The post-stishovite phase transition in hydrous alumina-bearing SiO_2 in the lower mantle of the earth. *Proceedings of the National Academy of Sciences of the United States of America* 104: 13588–13590.

Lay T, Garnero EJ, and Williams Q (2004) Partial melting in a thermo-chemical boundary layer at the base of the mantle. *Physics of the Earth and Planetary Interiors* 146: 441–467.

Lay T, Williams Q, and Garnero EJ (1998) The core-mantle boundary layer and deep Earth dynamics. *Nature* 394: 461–468.

Li B (2003) Compressive and shear wave velocities of ringoodite γ-Mg_2SiO_4 to 12 GPa. *American Mineralogist* 88: 1312–1317.

Li J, Struzhkin VV, Mao H-K, et al. (2004) Electronic spin state of iron in lower mantle perovskite. *Proceedings of the National Academy of Sciences* 101: 14027–14030.

Li L, Weidner DJ, Brodholt J, et al. (2006a) Elasticity of $CaSiO_3$ perovskite at high pressure and high temperature. *Physics of the Earth and Planetary Interiors* 155: 249–259.

Li L, Weidner DJ, Brodholt J, et al. (2006b) Phase stability of $CaSiO_3$ perovskite at high pressure and temperature: Insights from *ab initio* molecular dynamics. *Physics of the Earth and Planetary Interiors* 155: 260–268.

Lin J-F, Heinz DL, Mao H-K, et al. (2003) Stability of magnesiowüstite in earth's lower mantle. *Proceedings of the National Academy of Sciences* 100: 4405–4408.

Lin J-F, Speziale S, Mao Z, and Marquardt H (2013) Effects of electronic spin transitions of iron in lower mantle minerals: Implications for deep mantle geophysics. *Reviews of Geophysics* 51: 244–275.

Lin J-F, Struzhkin VV, Jacobsen SD, et al. (2005) Spin transition of iron in magnesiowüstite in the Earth's lower mantle. *Nature* 436: 377–380.

Lin J-F, Weir ST, Jackson DD, et al. (2007) Electrical conductivity of the lower-mantle ferropericlase across the electronic spin transition. *Geophysical Research Letters* 34. http://dx.doi.org/10.1029/2007GL030523.

Litasov K, Ohtani E, Sano A, Suzuki A, and Funakoshi K (2005) *In situ* X-ray diffraction study of post-spinel transformation in a peridotite mantle: Implication for the 660-km discontinuity. *Earth and Planetary Science Letters* 238: 311–328.

Liu L-G (1977) High pressure $NaAlSiO_4$: The first silicate calcium ferrite isotope. *Geophysical Research Letters* 4: 183–186.

Liu L-G (1978) A new high-pressure phase of spinel. *Earth and Planetary Science Letters* 41: 398–404.

Liu L-G (1982) Speculations on the composition and origin of the Earth. *Geochemical Journal* 16: 287–310.

Liu L-G (1986) Phase transformations in serpentine at high pressures and temperatures and implications for subducting lithosphere. *Physics of the Earth and Planetary Interiors* 42: 255–262.

Liu L-G (1999) Genesis of diamonds in the lower mantle. *Contributions to Mineralogy and Petrology* 134: 170–173.

Liu X (2006) Phase relations in the system $KAlSi_3O_8$–$NaAlSi_3O_8$ at high pressure-high temperature conditions and their implication for the petrogenesis of lingunite. *Earth and Planetary Science Letters* 246: 317–325.

Loubet M, Sassi R, and Di Donato G (1988) Mantle heterogeneities: A combined isotope and trace element approach and evidence for recycled continental crust materials in some OIB sources. *Earth and Planetary Science Letters* 89: 299–315.

Magyari-Köpe B, Vitos L, Grimvall G, Johansson B, and Kollár J (2002) Low-temperature crystal structure of $CaSiO_3$ perovskite: An *ab initio* total energy study. *Physical Review B* 65: 193107.

Mainprice D, Barruol G, and Ismail W (2000) From single crystal to polycrystal. In: Karato S-I, Forte AM, Liebermann RC, Masters G, and Stixrude L (eds.) *Eath's Deep Interior: Mineral Physics and Tomography from the Atomic to the Global Scale. AGU Monograph*, vol. 117, pp. 237–264. Washington, DC: American Geophysical Union.

Mao HK, Chen LC, Hemley RJ, Jephcoat AP, and Wu Y (1989) Stability and equation of state of $CaSiO_3$ up to 134 GPa. *Journal of Geophysical Research* 94: 17889–17894.

Mao HK, Hemley RJ, Fei Y, et al. (1991) Effect of pressure, temperature and composition on lattice parameters and density of (Fe, Mg)SiO_3-perovskites to 30 GPa. *Journal of Geophysical Research* 96: 8069–8080.

Mao WL, Meng Y, Shen G, et al. (2005) Iron-rich silicates in the Earth's D″ layer. *Proceedings of the National Academy of Sciences* 102: 9751–9753.

Mao WL, Shen G, Prakapenka VB, et al. (2004) Ferromagnesian postperovskite silicates in the D″ layer of the Earth. *Proceedings of the National Academy of Sciences* 101: 15867–15869.

Marquardt H, Speziale S, Reichmann HJ, Frost DJ, and Schilling FR (2009a) Single-crystal elasticity of $(Mg_{0.9}Fe_{0.1})O$ to 81 GPa. *Earth and Planetary Science Letters* 287: 345–352.

Marquardt H, Speziale S, Reichmann HJ, Frost DJ, Schilling FR, and Garnero EJ (2009b) Elastic shear anisotropy of ferropericlase in Earth's lower mantle. *Science* 324: 224–226.

Marton F and Cohen R (1994) Prediction of a high pressure phase transition in Al_2O_3. *American Mineralogist* 79: 789–792.

Matsui M and Nishiyama N (2002) Comparison between the Au and MgO pressure calibration standards at high temperature. *Geophysical Research Letters* 29: 1368. http://dx.doi.org/10.1029/2001GL014161.

Matsui M, Parker SC, and Leslie M (2000) The M simulation of the equation of state of MgO: Application as a pressure standard at high temperature and high pressure. *American Mineralogist* 85: 312–316.

Mattern E, Matas J, Ricard Y, and Bass J (2005) Lower mantle composition and temperature from mineral physics and thermodynamic modeling. *Geophysical Journal International* 160: 973–990.

Mazin II, Fei Y, Downs R, and Cohen R (1998) Possible polytypism in FeO at high pressures. *American Mineralogist* 83: 451–457.

McCammon C (1997) Perovskite as a possible sink for ferric iron in the lower mantle. *Nature* 387: 694–696.

Meade C, Mao HK, and Hu J (1995) High-temperature phase transition and dissociation of (Mg,Fe)SiO_3 perovskite at lower mantle pressures. *Science* 268: 1743–1745.

Merkel S, McNamara AK, Kubo A, et al. (2007) Deformation of (Mg,Fe)SiO_3 post-perovskite and D″ anisotropy. *Science* 316: 1729–1732.

Metsue A and Tsuchiya T (2011) Lattice dynamics and thermodynamic properties of $(Mg,Fe^{2+})SiO_3$ postperovskite. *Journal of Geophysical Research* 116. http://dx.doi.org/10.1029/2010JB008018.

Metsue A and Tsuchiya T (2012) Thermodynamic properties of $(Mg,Fe^{2+})SiO_3$ perovskite at the lower-mantle pressures and temperatures: an internally consistent LSDA+U study. *Geophysical Journal International* 190: 310–322.

Metsue A and Tsuchiya T (2013) Shear response of Fe-bearing $MgSiO_3$ post-perovskite at lower mantle pressures. *Proceedings of the Japan Academy Series B* 89: 51–58.

Michael PJ and Bonatti E (1985) Peridotite composition from the North Atlantic: Regional and tectonic variations and implications for partial melting. *Earth and Planetary Science Letters* 73: 91–104.

Mitchell BJ and Helmberger DV (1973) Shear velocities at the base of the mantle from observations of S and ScS. *Journal of Geophysical Research* 78: 6009–6020.

Miyagi L, Kanitpanyacharoen W, Kaercher P, Lee KKM, and Wenk H-R (2010) Slip system in $MgSiO_3$ post-perovskite: Implications for D″ anisotropy. *Science* 329: 1639–1641.

Miyagi L, Kanitpanyacharoen W, Stackhouse S, Militzer B, and Wenk H (2011) The enigma of post-perovskite anisotropy: Deformation versus transformation textures. *Physics and Chemistry of Minerals* 38: 665–678.

Miyajima N, Yagi T, Hirose K, Kondo T, Fujino K, and Miura H (2001) Potential host phase of aluminum and potassium in the Earth's lower mantle. *American Mineralogist* 86: 740–746.

Mookherjee M and Steinle-Neumann G (2009) Detecting deeply subducted crust from the elasticity of hollandite. *Earth and Planetary Science Letters* 288: 349–358.

Murakami M and Bass J (2011) Evidence of denser $MgSiO_3$ glass above 133 gigapascal (GPa) and implications for remnants of ultradense silicate melt from a deep magma ocean. *Proceedings of the National Academy of Sciences of the United States of America* 108: 17286–17289.

Murakami M, Hirose K, Kawamura K, Sata N, and Ohishi Y (2004a) Post-perovskite phase transition in $MgSiO_3$. *Science* 304: 855–858.

Murakami M, Hirose K, Ono S, Isshiki M, and Watanuki T (2004b) High pressure and high temperature phase transitions of FeO. *Physics of the Earth and Planetary Interiors* 146: 273–282.

Murakami M, Hirose K, Ono S, and Ohishi Y (2003) Stability of $CaCl_2$-type and α-PbO_2-type SiO_2 at high pressure and temperature determined by *in situ* X-ray measurements. *Geophysical Research Letters* 30. http://dx.doi.org/10.1029/2002GL016722.

Murakami M, Hirose K, Sata N, and Ohishi Y (2005) Post-perovskite phase transition and mineral chemistry in the pyrolitic lowermost mantle. *Geophysical Research Letters* 32. http://dx.doi.org/10.1029/2004GL021956, L03304.

Murakami M, Ohishi Y, Hirao N, and Hirose K (2012) A perovskitic lower mantle inferred from high-pressure, high-temperature sound velocity data. *Nature* 485: 90–94.

Nakagawa T and Tackley PJ (2004) Effects of a perovskite–post perovskite phase change near core-mantle boundary in compressible mantle convection. *Geophysical Research Letters* 31: L16611. http://dx.doi.org/10.1029/2004GL020648.

Nakagawa T, Tackley PJ, Deschamps F, and Connolly JAD (2010) The influence of MORB and harzburgite composition on thermo-chemical mantle convection in a 3-D spherical shell with self-consistently calculated mineral physics. *Earth and Planetary Science Letters* 296: 403–412.

Nishi M, Kubo T, Kato T, Tominaga A, Funakoshi K-I, and Higo Y (2011) Exsolution kinetics of majoritic garnet from clinopyroxene in subducting oceanic crust. *Physics of the Earth and Planetary Interiors* 189: 47–55.

Nishio-Hamane D, Fujino K, Seto Y, and Nagai T (2007) Effect of the incorporation of $FeAlO_3$ into $MgSiO_3$ perovskite on the post-perovskite transition. *Geophysical Research Letters* 34. http://dx.doi.org/10.1029/2007GL029991.

Nishiyama N, Irifune T, Inoue T, Ando J, and Funakoshi K (2004) Precise determination of phase relations in pyrolite across the 660 km seismic discontinuity by *in situ* X-ray diffraction and quench experiments. *Physics of the Earth and Planetary Interiors* 143–144: 185–199.

Nishiyama N and Yagi T (2003) Phase relation and mineral chemistry in pyrolite to 2200 C under the lower mantle pressures and implications for dynamics of mantle plumes. *Journal of Geophysical Research* 108(B5): 2255.

Niu F and Kawakatsu H (1996) Complex structure of the mantle discontinuities at the tip of the subducting slab beneath the northeast China: A preliminary investigation of broadband receiver functions. *Journal of Physics of the Earth* 44: 701–711.

Oganov AR, Gillan MJ, and Price GD (2005a) Structural stability of silica at high pressures and temperatures. *Physical Review B* 71: 064104.

Oganov AR, Martonak R, Laio A, Raiteri P, and Parrinello M (2005b) Anisotropy of Earth's D″ layer and stacking faults in the $MgSiO_3$ postperovskite phase. *Nature* 438: 1142–1144.

Oganov AR, Glass CW, and Ono S (2006) High-pressure phases of $CaCO_3$: Crystal structure prediction and experiment. *Earth and Planetary Science Letters* 241: 95–103.

Oganov AR and Ono S (2004) Theoretical and experimental evidence for a post-perovskite phase of $MgSiO_3$ in Earth's D″ layer. *Nature* 430: 445–448.

Oganov AR, Ono S, Ma Y, Glass CW, and Garcia A (2008) Novel high-pressure structures of $MgCO_3$, $CaCO_3$ and CO_2 and their role in Earth's lower mantle. *Earth and Planetary Science Letters* 273: 38–47.

Ohta K, Cohen RE, Hirose K, Haule K, Shimizu K, and Ohishi Y (2012) Experimental and theoretical evidence for the pressure-induced metallization in FeO with rocksalt-type structure. *Physical Review Letters* 108, Art. No. 026403.

Ohta K, Hirose K, Shimizu K, and Ohishi Y (2010) High-pressure experimental evidence for metal FeO with normal NiAs-type structure. *Physical Review B* 82: 174120.

Ohtani E, Kagawa N, and Fujino K (1991) Stability of majorite $(Mg,Fe)SiO_3$ at high pressures and 1800°C. *Earth and Planetary Science Letters* 102: 158–166.

Ohtani E, Litasov K, Hosoya T, Kubo T, and Kondo T (2004) Water transport into the deep mantle and formation of a hydrous transition zone. *Physics of the Earth and Planetary Interiors* 143–144: 255–269.

Ohtani E, Mizobata H, Kudoh Y, et al. (1997) A new hydrous silicate, a water reservoir, in the upper part of the lower mantle. *Geophysical Research Letters* 24: 1047–1050.

Okada T, Yagi T, Niwa K, and Kikegawa T (2010) Lattice-preferred orientations in post-perovskite-type $MgGeO_3$ formed by transformations from different pre-phases. *Physics of the Earth and Planetary Interiors* 180: 195–202.

Ono A, Akaogi M, Kojitani H, Yamashita K, and Kobayashi M (2009) High-pressure phase relations and thermodynamic properties of hexagonal aluminous phase and calcium-ferrite phase in the systems $NaAlSiO_4$–$MgAl_2O_4$ and $CaAl_2O_4$–$MgAl_2O_4$. *Physics of the Earth and Planetary Interiors* 174: 39–49.

Ono S, Funakoshi K, Ohishi Y, and Takahashi E (2005a) *In situ* X-ray observation of the phase transition of Fe_2O_3. *Journal of Physics: Condensed Matter* 17: 269–276.

Ono S, Kikegawa T, and Ohishi Y (2005b) A high-pressure and high-temperature synthesis of platinum carbide. *Solid State Communications* 133: 55–59.

Ono S, Kikegawa T, Ohishi Y, and Tsuchiya J (2005c) Post-aragonite phase transformation in $CaCO_3$ at 40 GPa. *American Mineralogist* 90: 667–671.

Ono S, Ohishi Y, Isshiki M, and Watanuki T (2005d) *In situ* X-ray observations of phase assemblages in peridotite and basalt compositions at lower mantle conditions: Implications for density of subducted oceanic plate. *Journal of Geophysical Research* 110: B02208. http://dx.doi.org/10.1029/2004JB003196.

Ono S, Ohishi Y, and Mibe K (2004) Phase transition of Ca-perovskite and stability of Al-bearing Mg-perovskite in the lower mantle. *American Mineralogist* 89: 1480–1485.

Ono S, Hirose K, Murakami M, and Isshiki M (2002) Post-stishovite phase boundary in SiO_2 determined by *in situ* X-ray observations. *Earth and Planetary Science Letters* 197: 187–192.

Ono S, Ito E, and Katsura T (2001) Mineralogy of subducted basaltic crust (MORB) from 25 to 37 GPa, and chemical heterogeneity of the lower mantle. *Earth and Planetary Science Letters* 190: 57–63.

Ono S, Kikegawa T, and Ohishi Y (2007) High-pressure transition of $CaCO_3$. *American Mineralogist* 92: 1246–1249.

Panero WR and Stixrude LP (2004) Hydrogen incorporation in stishovite at high pressure and symmetric hydrogen bonding in δ-AlOOH. *Earth and Planetary Science Letters* 221: 421–431.

Panning M and Romanowicz B (2004) Inference on flow at the base of Earth's mantle based on seismic anisotropy. *Science* 303: 351–353.

Parise JB, Wang Y, Yeganeh-Haeri A, Cox DE, and Fei Y (1990) Crystal structure and thermal expansion of $(Mg,Fe)SiO_3$ perovskite. *Geophysical Research Letters* 17: 2089–2092.

Perdew JP, Burke K, and Ernzerhof M (1996) Generalized gradient approximation made simple. *Physical Review Letters* 77: 3865–3868.

Perdew JP, Chevary JA, Vosko SH, et al. (1992) Atoms, molecules, solids, and surfaces: Applications of the generalized gradient approximation for exchange and correlation. *Physical Review B* 46: 6671–6687.

Rapp RP, Irifune T, Shimizu N, Nishiyama N, Norman MD, and Inoue T (2008) Subduction recycling of continental sediments and the origin of geochemically enriched reservoirs in the deep mantle. *Earth and Planetary Science Letters* 271: 14–23.

Ricolleau A, Fiquet G, Addad A, et al. (2008) Analytical transmission electron microscopy study of a natural MORB sample assemblage transformed at high pressure and high temperature. *American Mineralogist* 93: 144–153.

Ricolleau A, Perrillat J-P, Fiquet G, et al. (2010) Phase relations and equation of state of a natural MORB: Implications for the density profile of subducted oceanic crust in the Earth's lower mantle. *Journal of Geophysical Research* 115. http://dx.doi.org/10.1029/2009JB006709.

Ringwood AE (1962) A model for the upper mantle. *Journal of Geophysical Research* 67: 857–867.

Ringwood AE (1994) Role of the transition zone and 660 km discontinuity in mantle dynamics. *Physics of the Earth and Planetary Interiors* 86: 5–24.

Ringwood AE and Irifune T (1988) Nature of the 650-km seismic discontinuity: Implications for mantle dynamics and differentiation. *Nature* 331: 131–136.

Ringwood AE, Kato T, Hibberson W, and Ware N (1990) High-pressure geochemistry of Cr, V and Mn and implications for the origin of the moon. *Nature* 347: 174–176.

Ross NL and Hazen RM (1990) High-pressure crystal chemistry of $MgSiO_3$ perovskite. *Physics and Chemistry of Minerals* 17: 228–237.

Ross NL, Shu JF, Hazen M, and Gasparik T (1990) High-pressure crystal chemistry of stishovite. *American Mineralogist* 75: 739–747.

Sanehira T, Irifune T, Shinmei T, Brunet F, Funakoshi K, and Nozawa A (2005) *In situ* X-ray diffraction study of an aluminous phase in MORB under lower mantle conditions. *Physics and Chemistry of Minerals* 33: 28–34. http://dx.doi.org/10.1007/s00269-005-0043-0.

Sano A, Ohtani E, Kondo T, et al. (2008) Aluminous hydrous mineral δ-AlOOH as a carrier of hydrogen into the core-mantle boundary. *Geophysical Research Letters* 35. http://dx.doi.org/10.1029/2007GL031718.

Santillán J and Williams Q (2004) A high pressure X-ray diffraction study of aragonite and the post-aragonite phase transition in $CaCO_3$. *American Mineralogist* 89: 1348–1352.

Sawamoto H (1987) Phase diagram of $MgSiO_3$ at pressures up to 24 GPa and temperatures up to 2200°C: Phase stability and properties of tetragonal garnet. In: Manghnani MH and Syono Y (eds.) *High-Pressure Research in Mineral Physics*, pp. 209–219. Tokyo: Terrapub/American Geophysical Union.

Saxena SK, Dubrovinsky LS, Lazor P, et al. (1996) Stability of perovskite ($MgSiO_3$) in the earth's mantle. *Science* 274: 1357–1359.

Sharp TG, El Goresy A, Wopenka B, and Chen M (1999) A post-stishovite SiO_2 polymorph in the meteorite Shergotty: Implications for impact events. *Science* 284: 1511–1513.

Shen G, Rivers ML, Wang Y, and Sutton R (2001) Laser heated diamond anvil cell system at the advanced photon source for *in situ* X-ray measurements at high pressure and temperature. *Review of Scientific Instruments* 72: 1273–1282.

Sherman DM and Jansen H (1995) First-principles prediction of the high-pressure phase transition and electronic structure of FeO: Implications for the chemistry of the lower mantle and core. *Geophysical Research Letters* 22: 1001–1004.

Shieh SR, Duffy TS, and Li B (2002) Strength and elasticity of SiO_2 across the stishovite-$CaCl_2$-type structural phase boundary. *Physical Review Letters* 89: 255507.

Shieh SR, Duffy TS, and Shen G (2004) Elasticity and strength of calcium silicate perovskite at lower mantle pressures. *Physics of the Earth and Planetary Interiors* 143–144: 93–105.

Shieh SR, Mao H-K, Hemley RJ, and Ming LC (1998) Decomposition of phase D in the lower mantle and the fate of dense hydrous silicates in subducting slab. *Earth and Planetary Science Letters* 159: 13–23.

Shim S-H and Duffy TS (2000) Constraints on the P–V–T equation of state of $MgSiO_3$ perovskite. *American Mineralogist* 85: 354–363.

Shim S-H, Duffy TS, Jeanloz R, and Shen G (2004) Stability and crystal structure of $MgSiO_3$ perovskite to the core-mantle boundary. *Geophysical Research Letters* 31. http://dx.doi.org/10.1029/2004GL019639.

Shim S-H, Duffy TS, and Shen G (2000a) The stability and P–V–T equation of state of $CaSiO_3$ perovskite in the earth's lower mantle. *Journal of Geophysical Research* 105: 25955–25968.

Shim S-H, Duffy TS, and Shen G (2000b) The equation of state of $CaSiO_3$ perovskite to 108 GPa at 300 K. *Physics of the Earth and Planetary Interiors* 120: 327–338.

Shim S-H, Duffy TS, and Shen G (2001a) The post-spinel transformation in Mg_2SiO_4 and its relation to the 660-km seismic discontinuity. *Nature* 411: 571–573.

Shim S-H, Duffy TS, and Shen G (2001b) Stability and structure of $MgSiO_3$ perovskite to 2300-kilometer depth in earth's mantle. *Science* 293: 2437–2440.

Shim S-H, Duffy TS, and Takemura K (2002a) Equation of state of gold and its application to the phase boundaries near 660 km depth in the Earth's mantle. *Earth and Planetary Science Letters* 203: 729–739.

Shim S-H, Jeanloz R, and Duffy TS (2002b) Tetragonal structure of $CaSiO_3$ perovskite above 20 GPa. *Geophysical Research Letters* 29: 2166.

Shimomura O, Yamaoka S, Yagi T, et al. (1984) Multi-anvil type X-ray apparatus for synchrotron radiation. *Materials Research Society Symposia Proceedings*, vol. 22, pp. 17–20. Amsterdam: Elsevier.

Shinmei T, Sanehira T, Yamazaki D, et al. (2005) High-temperature and high-pressure equation of state for the hexagonal phase in the system $NaAlSiO_4$–$MgAl_2O_4$. *Physics and Chemistry of Minerals* 32: 594–602. http://dx.doi.org/10.1007/s00269-005-0029-y.

Sidorin I, Gurnis M, and Helmberger DV (1999) Evidence for a ubiquitous seismic discontinuity at the base of the mantle. *Science* 286: 1326–1331.

Simmons NA and Gurrola H (2000) Seismic evidence for multiple discontinuities near the base of the transition zone. *Nature* 405: 559–562.

Sinmyo R and Hirose K (2013) Iron partitioning in pyrolite lower mantle. *Physics and Chemistry of Minerals* 40: 107–113.

Sinmyo R, Hirose K, Muto S, Ohishi Y, and Yasuhara A (2011) The valence state and partitioning of iron in the Earth's lowermost mantle. *Journal of Geophysical Research* 116. http://dx.doi.org/10.1029/2010JB008179.

Sinmyo R, Hirose K, Nishio-Hamane D, et al. (2008) Partitioning of iron between perovskite/post-perovskite and ferropericlase in the lower mantle. *Journal of Geophysical Research* 113, Art. No. B11204.

Sinogeikin SV and Bass JD (2000) Single-crystal elasticity of pyrope and MgO to 20 GPa by Brillouin scattering in the diamond cell. *Physics of the Earth and Planetary Interiors* 120: 43–62.

Sinogeikin SV, Zhang J, and Bass JD (2004) Elasticity of single crystal and polycrystalline $MgSiO_3$ perovskite by Brillouin spectroscopy. *Geophysical Research Letters* 31: L06620. http://dx.doi.org/10.1029/2004GL019559.

Speziale S, Zha CS, Duffy TS, Hemley RJ, and Mao HK (2001) Quasi-hydrostatic compression of magnesium oxide to 52 GPa: Implications for the pressure–volume–temperature equation of state. *Journal of Geophysical Research* 106: 515–528. http://dx.doi.org/10.1029/2000JB900318.

Stacey FD and Isaak DG (2001) Compositional constraints on the equation of state and thermal properties of the lower mantle. *Geophysical Journal International* 146: 143–154.

Stackhouse S, Brodholt JP, and Price GD (2005a) High temperature elastic anisotropy of the perovskite and post-perovskite polymorphs of Al_2O_3. *Geophysical Research Letters* 32: L13305. http://dx.doi.org/10.1029/2005GL023163.

Stackhouse S, Brodholt JP, Wookey J, Kendall J-M, and Price GD (2005b) The effect of temperature on the seismic anisotropy of the perovskite and post-perovskite polymorphs of $MgSiO_3$. *Earth and Planetary Science Letters* 230: 1–10.

Stackhouse S, Brodholt JP, and Price GD (2006) Elastic anisotropy of $FeSiO_3$ end-members of the perovskite and post-perovskite phases. *Geophysical Research Letters* 33: L01304. http://dx.doi.org/10.1029/2005GL023887.

Stixrude L, Cohen RE, Yu R, and Krakauer H (1996) Prediction of phase transition in $CaSiO_3$ perovskite and implications for lower mantle structure. *American Mineralogist* 81: 1293–1296.

Stixrude L and Lithgow-Bertelloni C (2011) Thermodynamics of mantle minerals – II. Phase equilibria. *Geophysical Journal International* 184: 1180–1213.

Sueda Y, Irifune T, Nishiyama N, et al. (2004) A new high-pressure form of $KAlSi_3O_8$ under lower mantle conditions. *Geophysical Research Letters* 31: L23612. http://dx.doi.org/10.1029/2004GL021156.

Sun S (1982) Chemical composition and the origin of the Earth's primitive mantle. *Geochimica et Cosmochimica Acta* 46: 179–192.

Suzuki A, Ohtani E, and Kamada T (2000) A new hydrous phase δ-AlOOH synthesized at 21 GPa and 1000 °C. *Physics and Chemistry of Minerals* 27: 689–693.

Tackley PJ (2000) Mantle convection and plate tectonics: Toward an integrated physical and chemical theory. *Science* 288: 2002–2007.

Tamai H and Yagi T (1989) High-pressure. and high-temperature phase relations in $CaSiO_3$ and $CaMgSi_2O_6$ and elasticity of perovskite-type $CaSiO_3$. *Physics of the Earth and Planetary Interiors* 54: 370–377.

Tange Y, Irifune T, and Funakoshi K-I (2008) Pressure generation up to 80 GPa using multianvil apparatus with sintered diamond anvils. *High Pressure Research* 28: 245–254.

Tange Y, Kuwayama Y, Irifune T, Funakoshi K, and Ohishi Y (2012) P–V–T equation of state of $MgSiO_3$ perovskite based on the MgO pressure scale: A comprehensive reference for mineralogy of the lower mantle. *Journal of Geophysical Research* 117. http://dx.doi.org/10.1029/2011JB008988.

Tange Y, Nishihara Y, and Tsuchiya T (2009a) Unified analyses for P–V–T equation of state of MgO: A solution for pressure-scale problems in high P–T experiments. *Journal of Geophysical Research* 115. http://dx.doi.org/10.1029/2008JB005813.

Tange Y, Takahashi E, Nishihara Y, Funakoshi K, and Sata N (2009b) Phase relations in the system MgO–FeO–SiO_2 to 50 GPa and 2000 °C: An application of experimental techniques using multianvil apparatus with sintered diamond anvils. *Journal of Geophysical Research* 114. http://dx.doi.org/10.1029/2008JB05891.

Tateno S, Hirose K, Ohishi Y, and Tatsumi Y (2010) The structure of iron in Earth's inner core. *Science* 15: 359–361.

Tateno S, Hirose K, Sata N, and Ohishi Y (2005) Phase relations in $Mg_3Al_2Si_3O_{12}$ to 180 GPa: Effect of Al on post-perovskite phase transition. *Geophysical Research Letters* 32: L15306. http://dx.doi.org/10.1029/2005GL023309.

Tateno S, Hirose K, Sata N, and Ohishi Y (2007) Solubility of FeO in $(Mg,Fe)SiO_3$ perovskite and post-perovskite phase transition. *Physics of the Earth and Planetary Interiors* 160: 319–325.

Taylor SR and McLennan SM (1985) *The Continental Crust: Its Composition and Evolution*, pp. 312. Oxford: Blackwell.

Thomson KT, Wentzcovitch RM, and Bukowinski M (1996) Polymorphs of alumina predicted by first principles. *Science* 274: 1880–1882.

Tomioka N, Mori H, and Fujino K (2000) Shock-induced transition of $NaAlSi_3O_8$ feldspar into a hollandite structure in a L6 chondrite. *Geophysical Research Letters* 27: 3997–4000.

Torii Y and Yoshioka S (2007) Physical conditions producing slab stagnation: Constrants of the Clapeyron slope, mantle viscosity, trench retreat, and dip angles. *Tectonophysics* 445: 200–209.

Trampert T, Deschamps F, Resovsky J, and Yuen D (2004) Probabilistic tomography maps chemical heterogeneities throughout the lower mantle. *Science* 306: 853–856.

Tsuchiya T (2003) First-principles prediction of the P–V–T equation of state of gold and the 660-km discontinuity in Earth's mantle. *Journal of Geophysical Research* 108: 2462. http://dx.doi.org/10.1029/2003JB002446.

Tsuchiya T (2011) Elasticity of subducted basaltic crust at the lower mantle pressures: Insights on the nature of deep mantle heterogeneity. *Physics of the Earth and Planetary Interiors* 188: 142–149.

Tsuchiya J (2013) First principles prediction of a new high pressure phase of dense hydrous magnesium silicates in the lower mantle. *Geophysical Research Letters* 40: 4570–4573. http://dx.doi.org/10.1002/grl.50875.

Tsuchiya T, Caracas R, and Tsuchiya J (2004a) First principles determination of the phase boundaries of high-pressure polymorphs of silica. *Geophysical Research Letters* 31: L11610. http://dx.doi.org/10.1029/2004GL019649.

Tsuchiya T, Tsuchiya J, Umemoto K, and Wentzcovitch RM (2004b) Phase transition in $MgSiO_3$ perovskite in the Earth's lower mantle. *Earth and Planetary Science Letters* 224: 241–248.

Tsuchiya T, Tsuchiya J, Umemoto K, and Wentzcovitch RM (2004c) Elasticity of post-perovskite $MgSiO_3$. *Geophysical Research Letters* 31: L14603. http://dx.doi.org/10.1029/2004GL020278.

Tsuchiya T and Kawamura K (2001) Systematics of elasticity: *Ab initio* study in B1-type alkaline earth oxides. *Journal of Chemical Physics* 114: 10086–10093.

Tsuchiya T and Tsuchiya J (2006) Effect of impurity on the elasticity of perovskite and postperovskite: Velocity contrast across the postperovskite transition in (Mg, Fe, Al)(Si, Al)O_3. *Geophysical Research Letters* 33: L12S04. http://dx.doi.org/10.1029/2006GL025706.

Tsuchiya J and Tsuchiya T (2008) Post-perovskite phase equilibria in the $MgSiO_3$–Al_2O_3 system. *Proceedings of the National Academy of Sciences of the United States of America* 105: 19160–19164.

Tsuchiya J and Tsuchiya T (2011a) First-principles prediction of a high-pressure hydrous phase of AlOOH. *Physical Review B* 83. http://dx.doi.org/10.1103/PhysRevB.83.054115.

Tsuchiya T and Tsuchiya J (2011b) Prediction of a hexagonal SiO_2 phase affecting stabilities of $MgSiO_3$ and $CaSiO_3$ at multimegabar pressures. *Proceedings of the National Academy of Sciences of the United States of America* 108: 1252–1255.

Tsuchiya J, Tsuchiya T, and Tsuneyuki S (2002) First principles calculation of a high-pressure hydrous phase, δ-AlOOH. *Geophysical Research Letters* 29: 1909.

Tsuchiya J, Tsuchiya T, and Tsuneyuki S (2005a) First-principles study of hydrogen bond symmetrization of phase D under pressure. *American Mineralogist* 90: 44–49.

Tsuchiya J, Tsuchiya T, and Wentzcovitch RM (2005b) Vibrational and thermodynamic properties of $MgSiO_3$ postperovskite. *Journal of Geophysical Research* 110: B02204. http://dx.doi.org/10.1029/2004JB003409.

Tsuchiya J, Tsuchiya T, and Wentzcovitch RM (2005c) Transition from the Rh_2O_3(II)-to-$CaIrO_3$ structure and the high-pressure–temperature phase diagram of alumina. *Physical Review B* 72: 020103(R). http://dx.doi.org/10.1103/PhysRevB.72.020103.

Tsuchiya T and Wang X (2013) *Ab initio* investigation on the high-temperature thermodynamic properties of Fe^{3+}-bearing $MgSiO_3$ perovskite. *Journal of Geophysical Research* 118. http://dx.doi.org/10.1029/2012JB009696.

Tsuchiya T, Wentzcovitch RM, and de Gironcoli S (2006) Spin transition in Magnesiowüstite in Earth's lower mantle. *Physical Review Letters* 96: 198501.

Tutti F, Dubrovinsky LS, and Saxena SK (2000) High pressure phase transformation of jadeite and stability of $NaAlSiO_4$ with calcium-ferrite type structure in the lower mantle conditions. *Geophysical Research Letters* 27: 2025–2028.

Tutti F, Dubrovinsky LS, Saxena SK, and Carlson S (2001) Stability of $KAlSi_3O_8$ hollandite-type structure in the Earth's lower mantle conditions. *Geophysical Research Letters* 28: 2735–2738.

Umemoto K, Wentzcovitch RM, and Allen PB (2006) Dissociation of $MgSiO_3$ in the cores of gas giants and terrestrial exoplanets. *Science* 311: 983–986.

Van der Hilst R, Widiyantoro S, and Engdahl E (1997) Evidence for deep mantle circulation from global tomography. *Nature* 386: 578–584.

Vinnik L, Breger L, and Romanowicz B (1998) Anisotropic structures at the base of the Earth's mantle. *Nature* 393: 564–567.

Vinnik L, Kato M, and Kawakatsu H (2001) Search for seismic discontinuities in the lower mantle. *Geophysical Journal International* 147: 41–56.

Wallace DC (1972) *Thermodynamics of Crystals*. New York: Wiley, 484 pp.

Wang W and Takahashi E (1999) Subsolidus and melting experiments of a K-rich basaltic composition to 27 GPa: Implication for the behavior of potassium in the mantle. *American Mineralogist* 84: 357–361.

Wang Y, Uchida T, Von Dreele R, et al. (2004) A new technique for angle-dispersive powder diffraction using an energy-dispersive setup and synchrotron radiation. *Journal of Applied Crystallography* 37: 947–956.

Wang Y, Weidner DJ, and Guyot F (1996) Thermal equation of state of $CaSiO_3$ perovskite. *Journal of Geophysical Research* 101: 661–672.

Weidner DJ and Wang Y (2000) Phase transformations: Implications for mantle structure. In: Karato S, Forte AM, Liebermann RC, Masters G, and Stixrude L (eds.) *Geophysical Monograph*, vol. 117, pp. 215–235. Washington, DC: American Geophysical Union.

Wentzcovitch RM, Justo JF, Wu Z, da Silva CRS, Yuen DA, and Kohlstedt D (2009) Anomalous compressibility of ferropericlase throughout the iron spin cross-over. *Proceedings of the National Academy of Sciences of the United States of America* 106: 8447–8452.

Wentzcovitch RM, Ross NL, and Price GD (1995) *Ab initio* study of $MgSiO_3$ and $CaSiO_3$ perovskites at lower-mantle pressures. *Physics of the Earth and Planetary Interiors* 90: 101–112.

Wentzcovitch RM, Stixrude L, Karki BB, and Kiefer B (2004) Akimotoite to perovskite phase transition in $MgSiO_3$. *Geophysical Research Letters* 31: L10611. http://dx.doi.org/10.1029/2004GL019704.

Wentzcovitch RM, Tsuchiya T, and Tsuchiya J (2006) $MgSiO_3$ postperovskite at D″ conditions. *Proceedings of the National Academy of Sciences of the United States of America* 103: 543–546.

Wicks JK, Jackson JM, and Sturhahn W (2010) Very low velocities in iron-rich (Mg,Fe)O: Implications for the core-mantle boundary region. *Geophysical Research Letters* 37. http://dx.doi.org/10.1029/2010GL043689.

Williams Q (1998) The temperature contrast across D. In: Gurnis M, Wysession ME, Knittle E, and Buffett BA (eds.) *The Core-Mantle Boundary Region*, pp. 73–81. Washington, DC: American Geophysical Union.

Wood BJ (2000) Phase transitions and partitioning relations in peridotite under lower mantle conditions. *Earth and Planetary Science Letters* 174: 341–354.

Wood BJ and Rubie DC (1996) The effect of alumina on phase transformations at the 660-kilometer discontinuity from Fe–Mg partitioning experiments. *Science* 273: 1522–1524.

Wookey J, Stackhouse S, Kendall J-M, Brodholt JP, and Price GD (2005) Efficacy of the post-perovskite phase as an explanation of lowermost mantle seismic properties. *Nature* 438: 1004–1008.

Wysession ME, Lay T, Revenaugh J, et al. (1998) The D″ discontinuity and its implications. In: Gurnis M, Wysession ME, Knittle E, and Buffett BA (eds.) *The Core-Mantle Boundary Region*, pp. 273–298. Washington, DC: American Geophysical Union.

Yagi T, Mao HK, and Bell PM (1982) Hydrostatic compression of perovskite-type $MgSiO_3$. In: Saxena K (ed.) *Advances on Physical Geochemistry*, vol. 2, pp. 317–325. New York: Springer-Verlag.

Yagi T, Suzuki T, and Akaogi M (1994) High pressure transitions in the system $KAlSi_3O_8$–$NaAlSi_3O_8$. *Physics and Chemistry of Minerals* 21: 387–391.

Yamazaki D and Karato S (2002) Fabric development in (Mg,Fe)O during large strain, shear deformation: Implications for seismic anisotropy in Earth's lower mantle. *Physics of the Earth and Planetary Interiors* 131: 251–267.

Yang H, Prewitt CT, and Frost DJ (1997) Crystal structure of the dense hydrous magnesium silicate, phase D. *American Mineralogist* 82: 651–654.

Yeganeh-Haeri A, Weidner DJ, and Ito E (1989) Elasticity of $MgSiO_3$ in the perovskite structure. *Science* 248: 787–789.

Yu YG, Wentzcovitch RM, Tsuchiya T, Umemoto K, and Tsuchiya J (2006) First principles investigation of Ringwoodite's dissociation. *Geophysical Research Letters* 34. http://dx.doi.org/10.1029/2007GL029462.

Zhao D (2004) Global tomographic images of mantle plumes and subducting slabs: Insight into deep Earth dynamics. *Physics of the Earth and Planetary Interiors* 146: 3–34.

Zhou C, Greaux S, Nishiyama N, Irifune T, and Higo Y (2013) Sound velocities measurement on $MgSiO_3$ akimotoite at high pressures and high temperatures with simultaneous in situ X-ray diffraction and ultrasonic study. *Physics of the Earth and Planetary Interiors*. http://dx.doi.org/10.1016/j.pepi.2013.06.005.